Neutrino Reactions on Deuteron

S. Nakamura[1], T. Sato[1,2], V. Gudkov[2] and K. Kubodera[2]

[1] *Department of Physics, Osaka University, Toyonaka, Osaka 560-0043, Japan*

[2] *Department of Physics and Astronomy, University of South Carolina, Columbia, SC 29208, USA*

ABSTRACT

The cross sections for the $\nu-d$ and $\bar{\nu}-d$ reactions are calculated for the incident energy up to $E_\nu = 170$ MeV, with the use of a phenomenological Lagrangian approach. We assess and improve the reliability of the employed calculational method by examining the dependence of the results on various input and approximations that go into the calculation. The main points of improvements over the existing work are: (1) use of the "modern" NN potentials; (2) use of the more accurate nucleon weak-interaction form factors; (3) monitoring the strength of a vertex that governs the exchange-current contribution, with the use of data on the related process, $n+p \to d+\gamma$. In addition to the total cross sections, we present various differential cross sections that are expected to be useful for the SNO and other experiments. In the low energy regime relevant to the solar neutrinos, the newly calculated total cross sections agree with the existing literature values. The origins of slight differences found for higher energies are discussed.

I. INTRODUCTION

The neutrino-deuterium reactions[1] have been studied extensively over the past decades [1–12]. Recent detailed studies are strongly motivated by the proposal and successful start of the Sudbury Neutrino Observatory (SNO) [13], which uses a large underground heavy-water Cerenkov counter. One of the primary goals of SNO is to study the solar neutrinos by monitoring three reactions occurring in heavy water: (i) $\nu - e$ scattering, $\nu_e + e^- \rightarrow \nu_e + e^-$; (ii) the charged-current (CC) reaction, $\nu_e + d \rightarrow e^- + p + p$; (iii) the neutral-current (NC) reaction, $\nu_x + d \rightarrow \nu_x + n + p$, where ν_x stands for a neutrino of any flavor. The unique feature of SNO is its ability to register the CC and NC reactions separately but simultaneously. Since the NC reaction measures the total flux of the solar neutrinos (regardless of their flavors), SNO experiments offer valuable information about the nature of possible neutrino oscillation. SNO is also capable of monitoring astrophysical neutrinos the energy of which extends well beyond the solar neutrinos energy regime, a prominent example being supernova neutrinos. Obviously, in interpreting experimental results to be obtained at SNO, the accurate knowledge of the $\nu-d$ reaction cross sections is a prerequisite. Although the $\nu - e$ scattering cross section is readily available from the standard model, estimation of the neutrino-deuteron reaction cross sections requires a detailed examination of the structure of two-nucleon systems and their responses to electroweak probes.

In describing the current theoretical situation regarding the $\nu-d$ cross sections, it is useful to consider the $\nu - d$ reactions in a broader context of the general responses of two-nucleon systems to electroweak probes. A highly successful method for describing these responses is to consider one-body impulse approximation terms and two-body exchange-current terms acting on non-relativistic nuclear wave functions, with the exchange currents derived from a one-boson exchange model. In a modern realization of this approach [14–16], the vertices

[1]When convenient, we use the word "neutrino" and the symbol "ν" in a generic sense, referring to both neutrinos and anti-neutrinos.

characterizing relevant Feynman diagrams are determined, as much as possible, with the use of the low-energy theorems and current algebra. Some coupling constants are inferred from models (the quark model, SU(3), SU(6), etc.). In the present work we refer to this type of formalism as the phenomenological Lagrangian approach (PhLA). This formalism has been used extensively for electromagnetic processes in two nucleon systems [17–19]. The reported good agreement between theory and experiment gives a strong hint of the basic soundness of PhLA. This method has also been applied to two-nucleon weak-interaction processes such as muon capture on the deuteron [6,20,21], the *pp*-fusion reaction [20,22], and the $\nu - d$ reactions. For the muon capture, the calculated capture rate agrees reasonably well with the experimental value, again rendering support for the basic legitimacy of PhLA. (For the *pp* fusion there is unfortunately no data available.)

For the neutrino-deuterium reactions, the most detailed study within the framework of the impulse approximation (IA) has been done by Ying, Henley and Haxton (YHH) [8], while the most elaborate PhLA calculations including the exchange-current effects as well as the IA terms have been carried out in [6–9], and the latest status is described in [10], to be referred to as KN.[2] In the solar neutrino energy regime, the cross sections given in KN are slightly larger than those of YHH. This difference, however, is mostly due to the absence of the exchange-current contributions in YHH. As far as comparison with data is concerned, Tatara *et al.*'s estimate [6] of $\sigma(\nu_e + d \to e^- + p + p)$ averaged over the Michel spectrum of ν_e agrees with the result of a stopped-pion-beam experiment [23] within large experimental errors (30%). Furthermore, the result of a Bugey reactor neutrino experiment [24] agrees, within 10% experimental errors, with the values of $\sigma(\bar{\nu}_e + d \to e^+ + n + n)$ and $\sigma(\bar{\nu}_e + d \to \bar{\nu}_e + p + n)$ given in KN. Thus PhLA seems to provide a reasonably reliable framework for calculating the neutrino-deuteron cross sections.

---

[2]Ref. [10] also gives a rather detailed account of the relation between these latest calculations and the earlier work.

Meanwhile, a new approach based on effective field theory (EFT) has been scoring great success in describing low-energy electroweak processes in the two-nucleon systems [25–30]. In particular, the rate of thermal neutron radiative capture on the proton ($n + p \to d + \gamma$) has been calculated in chiral perturbation theory (χPT) and the result is found to be in perfect agreement with the data [25]. Butler and Chen [11] and Butler, Chen and Kong [12] have recently made extremely elaborate studies of $\nu - d$ cross sections for the solar neutrino energies with the use of EFT. The results of their EFT calculation agree with those of PhLA in the following sense. In an EFT approach, one starts with a general effective Lagrangian, $\mathcal{L}_{eff}$, that contains all possible terms compatible with given symmetries and a given order of expansion; the coefficient of each term in $\mathcal{L}_{eff}$ is called the low-energy coefficient (LEC). Now, it often happens that some LEC's cannot be fixed by the symmetry requirements alone and hence need to be treated as parameters to be determined empirically. In [11,12], the coefficient $L_{1\mathrm{A}}$ of a four-nucleon axial-current counter term enters as an unknown parameter, although dimensional arguments suggest $-6\,\mathrm{fm}^3 \leq L_{1\mathrm{A}} \leq +6\,\mathrm{fm}^3$. According to [11], the $\bar{\nu}-d$ cross sections obtained in EFT agree very well with those of the PhLA calculation (YHH or KN), provided $L_{1\mathrm{A}}$ is adjusted appropriately. The optimal value of $L_{1\mathrm{A}}$ is $L_{1\mathrm{A}} = 6.3\,\mathrm{fm}^3$ for YHH, and $L_{1\mathrm{A}} = 1.0\,\mathrm{fm}^3$ for KN, reasonable values as compared with the above-mentioned dimensional estimates. The fact that an *ab initio* calculation (modulo one free parameter) based on EFT is consistent with the results of PhLA provides further evidence for the basic reliability of PhLA.

Bahcall, Krastev and Smirnov [31] have recently studied in great detail the consequences of measurements of various observables at SNO. As input for their analysis, the ν_e-d reaction cross sections of YHH and KN are used, and the difference between these two calculations are assumed to represent 1σ theoretical errors. According to [31], uncertainties in the $\nu - d$ cross sections represent the largest ambiguity in most physics conclusions obtainable from the SNO observables, a feature that again points to the importance of reducing the uncertainty in the $\nu - d$ reaction cross sections.

In the present article we carry out, within the framework of PhLA, a detailed study of the

cross sections for the charged-current (CC) and neutral-current (NC) reactions of neutrinos and anti-neutrinos with the deuteron:

$$\nu_e + d \to e^- + p + p, \tag{1}$$

$$\nu_x + d \to \nu_x + p + n \qquad (x = e,\ \mu,\ \text{or}\ \tau), \tag{2}$$

$$\bar{\nu}_e + d \to e^+ + n + n, \tag{3}$$

$$\bar{\nu}_x + d \to \bar{\nu}_x + p + n \qquad (x = e,\ \mu,\ \text{or}\ \tau)\,. \tag{4}$$

It is our view that, in calculating the low-energy $\nu - d$ cross sections, EFT and PhLA play complementary roles. EFT, being a general framework, is capable of giving model-independent results, *provided* all the LEC's in an effective Lagrangian $\mathcal{L}_{eff}$ are predetermined. At present, however, $\mathcal{L}_{eff}$ does contain an unknown LEC, L_{1A}.[3] Meanwhile, although PhLA is a model approach, its basic idea and the parameters contained in it have been tested using many observables. Thus, insofar as one accepts the validity of these tests, PhLA has predictive power. It is reassuring that, as mentioned, there is highly quantitative correspondence [11,12] between the low-energy $\nu - d$ cross sections obtained in PhLA and those of EFT within a reasonable range for L_{1A}. In this article we wish to investigate several key aspects of PhLA in more depth than hitherto reported.

Beyond the solar neutrino energy regime, PhLA is at present the only available formalism for evaluating the $\nu - d$ cross sections. The EFT calculation in [11,12], by design, "integrates out" all the degrees of freedom but that of the heavy baryon. The nature of this so-called "nucleon-only" EFT limits its applicability to very low incident neutrino energies (typically the solar neutrino energies).[4] On the other hand, there is no obvious conceptual

---

[3] In principle, however, it is possible to fix L_{1A} using a parity-violating electron scattering experiment. [11,12]

[4] One can hope to extend the applicability of EFT to higher energies by including the pion degree of freedom explicitly via χPT. An *ab initio* calculation based on χPT for the $\nu - d$ reactions is yet

obstacle in using PhLA in an energy regime significantly higher than that of the solar neutrinos. Therefore, once the reliability of PhLA is tested at low energies by comparison with experimental data or with the results of EFT, it is rather natural to use PhLA for higher energies as well. In this sense, too, EFT and PhLA seem to play complementary roles (at least, in the current status of the matter).

Our main goals here is to assess and improve the reliability of the PhLA calculation of the $\nu - d$ reaction cross sections, by carefully examining the dependence of the results on various input and approximations that go into calculations. The main points of improvements in this work over the existing estimates are: (1) Use of the "modern" NN potentials; (2) Use of the more accurate nucleon weak-interaction form factors; (3) Monitoring the strength of the $\pi N\Delta$ vertex that governs by far the dominant exchange-current contribution, with the use of data on the related process, $n + p \rightarrow d + \gamma$. A second practical goal of this paper is to provide detailed information about the various differential cross sections for the $\nu - d$ reactions. Although the total cross sections are well documented in the literature, there have not been systematic descriptions of the differential cross sections. We therefore discuss in detail the energy spectrum, angular distribution and double differential cross sections of the final lepton in the CC reaction and also the energy spectrum and angular distribution of the final neutron in the NC reaction. It is hoped that, the detailed information given here on these differential cross sections will be useful in analyzing SNO and other experiments.

In the low energy regime relevant to the solar neutrinos, our results are found to agree very well with those of KN. We argue that this and additional results reported in this article allow us to assign smaller theoretical errors to the $\nu - d$ cross sections than assumed by Bahcall *et al.* [31]. For higher energies, the present calculation gives $\nu - d$ total cross sections larger than those of KN by up to 6%; we shall discuss the origin of this variance.

The organization of the rest of this article is as follows. After giving in Sec. II a brief

---

to be done.

account of the general framework of our PhLA, we describe in Sec. III the calculational details, including the multipole expansion of the nuclear currents, and expressions for the cross sections for $\nu - d$ reactions. The numerical results are presented in Sec. IV, and discussion and summary are given in Sec. V. Some kinematical formulae necessary for calculating phase space integrals are given in Appendix.

II. FORMALISM

We are concerned with the $\nu/\bar{\nu} - d$ reactions listed in Eq.(1)-Eq.(4). The four-momenta of the participating particles are labeled as

$$\nu/\bar{\nu}(k) + d(P) \to \ell(k') + N_1(p'_1) + N_2(p'_2), \tag{5}$$

where ℓ corresponds to $e^{\pm}$ for the CC reactions [Eqs.(1),(3)], and to ν or $\bar{\nu}$ for the NC reactions [Eqs.(2),(4)]. The energy-momentum conservation reads $k + P = k' + P'$ with $P' \equiv p'_1 + p'_2$, and we denote a momentum transfer from lepton to nucleus by $q^\mu = k^\mu - k'^\mu = P'^\mu - P^\mu$. In the laboratory system to be used throughout this work, we write

$$k^\mu = (E_\nu, \boldsymbol{k}),\ k'^\mu = (E'_\ell, \boldsymbol{k}'),\ P^\mu = (M_d, \boldsymbol{0}),\ P'^\mu = (P'^0, \boldsymbol{P}'),\ q^\mu = (\omega, \boldsymbol{q}). \tag{6}$$

The interaction Hamiltonian for semileptonic weak processes is given by the product of the hadron current (J_λ) and the lepton current (L^λ) as[5]

$$H_W^{CC} = \frac{G_F \cos\theta_C}{\sqrt{2}} \int d\boldsymbol{x} [J_\lambda^{CC}(\boldsymbol{x}) L^\lambda(\boldsymbol{x}) + \text{h. c.}] \tag{7}$$

for the CC process and

$$H_W^{NC} = \frac{G_F}{\sqrt{2}} \int d\boldsymbol{x}\ [J_\lambda^{NC}(\boldsymbol{x}) L^\lambda(\boldsymbol{x}) + \text{h. c.}] \tag{8}$$

---

[5]Throughout we use the Bjorken and Drell convention for the metric and Dirac matrices, except that we adopt the Dirac spinor normalized as $u^\dagger u = 1$.

for the NC process. Here $G_F = 1.166 \times 10^{-5}$ GeV^{-2} is the Fermi coupling constant, and $\cos\theta_C = 0.9749$ is the Cabibbo angle.

The lepton current is given by

$$L^\lambda(\boldsymbol{x}) = \bar{\psi}_l(\boldsymbol{x})\gamma^\lambda(1-\gamma^5)\psi_\nu(\boldsymbol{x}), \tag{9}$$

and its matrix element is written as

$$\begin{aligned} l^\lambda \equiv < k'|L^\lambda(0)|k > &= \bar{u}_l(k')\gamma^\lambda(1-\gamma^5)u_\nu(k) \qquad \text{for } \nu-\text{reaction}\,, \\ &= \bar{v}_{\bar{\nu}}(k)\gamma^\lambda(1-\gamma^5)v_{\bar{l}}(k') \qquad \text{for } \bar{\nu}-\text{reaction}\,. \end{aligned} \tag{10}$$

The hadronic charged current has the form

$$J^{CC}_\lambda(\boldsymbol{x}) = V^\pm_\lambda(\boldsymbol{x}) + A^\pm_\lambda(\boldsymbol{x}), \tag{11}$$

where V_λ and A_λ denote the vector and axial-vector currents, respectively. The superscript $+(-)$ denotes the isospin raising (lowering) operator for the $\bar{\nu}(\nu)$-reaction. Meanwhile, according to the standard model, the hadronic neutral current is given by

$$J^{NC}_\lambda(\boldsymbol{x}) = (1-2\sin^2\theta_W)V^3_\lambda + A^3_\lambda - 2\sin^2\theta_W V^s_\lambda, \tag{12}$$

where θ_W is the Weinberg angle with $\sin^2\theta_W = 0.2312$. V^s_λ is the isoscalar part of the vector current, and the superscript '3' denotes the third component of the isovector current. In the present case the hadron current consists of one-nucleon impulse approximation (IA) terms and two-body meson exchange current (MEX) terms. Their explicit forms are described in the next subsections.

A. Impulse approximation current

The IA current is determined by the single-nucleon matrix elements of J_λ. The nucleon matrix elements of the currents are written as

$$< N(p') \mid V^\pm_\lambda(0) \mid N(p) > = \bar{u}(p')[f_V\gamma_\lambda + i\frac{f_M}{2M_N}\sigma_{\lambda\rho}q^\rho]\tau^\pm u(p), \tag{13}$$

$$< N(p') \mid A^\pm_\lambda(0) \mid N(p) > = \bar{u}(p')[f_A\gamma_\lambda\gamma^5 + f_P\gamma^5 q_\lambda]\tau^\pm u(p)\,, \tag{14}$$

where M_N is the average of the masses of the final two nucleons. For the third component of the isovector current, we simply replace $\tau^{\pm}$ with $\frac{\tau^3}{2}$. For the isoscalar current

$$< N(p') \mid V^s_\lambda(0) \mid N(p) > \; = \bar{u}(p')[f_V\gamma_\lambda + i\frac{f^s_M}{2M_N}\sigma_{\lambda\rho}q^\rho]\frac{1}{2}u(p). \tag{15}$$

The non-relativistic forms of the IA currents are given by

$$V^{\pm}_{IA,0}(\boldsymbol{x}) = \sum_i f_V\tau^{\pm}_i\delta(\boldsymbol{x}-\boldsymbol{r}_i), \tag{16}$$

$$\boldsymbol{V}^{\pm}_{IA}(\boldsymbol{x}) = \sum_i [f_V\frac{\boldsymbol{p}'_i+\boldsymbol{p}_i}{2M_N} + \frac{f_V+f_M}{2M_N}\boldsymbol{\nabla}\times\boldsymbol{\sigma}_i]\tau^{\pm}_i\delta(\boldsymbol{x}-\boldsymbol{r}_i), \tag{17}$$

$$A^{\pm}_{IA,0}(\boldsymbol{x}) = \sum_i [\frac{f_A}{2M_N}\boldsymbol{\sigma}_i\cdot(\boldsymbol{p}'_i+\boldsymbol{p}_i) - \frac{if_P\omega}{2M_N}\boldsymbol{\sigma}_i\cdot\boldsymbol{\nabla}]\tau^{\pm}_i\delta(\boldsymbol{x}-\boldsymbol{r}_i), \tag{18}$$

$$\boldsymbol{A}^{\pm}_{IA}(\boldsymbol{x}) = \sum_i [f_A\boldsymbol{\sigma}_i + \frac{f_P}{2M_N}\boldsymbol{\nabla}(\boldsymbol{\nabla}\cdot\boldsymbol{\sigma}_i)]\tau^{\pm}_i\delta(\boldsymbol{x}-\boldsymbol{r}_i), \tag{19}$$

$$V^s_{IA,0}(\boldsymbol{x}) = \sum_i f_V\;\frac{1}{2}\;\delta(\boldsymbol{x}-\boldsymbol{r}_i), \tag{20}$$

$$\boldsymbol{V}^s_{IA}(\boldsymbol{x}) = \sum_i [f_V\frac{\boldsymbol{p}'_i+\boldsymbol{p}_i}{2M_N} + \frac{f_V+f^s_M}{2M_N}\boldsymbol{\nabla}\times\boldsymbol{\sigma}_i]\;\frac{1}{2}\;\delta(\boldsymbol{x}-\boldsymbol{r}_i). \tag{21}$$

It is useful to rewrite $\boldsymbol{p}_i+\boldsymbol{p}'_i = \boldsymbol{q}+\boldsymbol{P}\pm 2\boldsymbol{p}_N$, where the $+(-)$ sign corresponds to $i=1$ $(i=2)$, and the derivative operator $\boldsymbol{p}_N$ should act on the deuteron wave function; in the laboratory system we are working in, we have $\boldsymbol{P}=\boldsymbol{0}$.

As for the q^2_μ dependence of the form factors we use the results of the latest analyses in [32,33]:

$$f_V(q^2_\mu) = G_D(q^2_\mu)(1+\mu_p\eta)(1+\eta)^{-1}, \tag{22}$$

$$f_M(q^2_\mu) = G_D(q^2_\mu)(\mu_p-\mu_n-1-\mu_n\eta)(1+\eta)^{-1}, \tag{23}$$

$$f_A(q^2_\mu) = -1.254\;G_A(q^2_\mu), \tag{24}$$

$$f_P(q^2_\mu) = \frac{2M_N}{m^2_\pi - q^2_\mu}f_A(q^2_\mu), \tag{25}$$

$$f^s_M(q^2_\mu) = G_D(q^2_\mu)(\mu_p+\mu_n-1+\mu_n\eta)(1+\eta)^{-1}, \tag{26}$$

with

$$G_D(q^2_\mu) = \left(1-\frac{q^2_\mu}{0.71\mathrm{GeV}^2}\right)^{-2}, \tag{27}$$

$$G_A(q^2_\mu) = \left(1-\frac{q^2_\mu}{1.14\mathrm{GeV}^2}\right)^{-2}, \tag{28}$$

where $\mu_p = 2.793$, $\mu_n = -1.913$, $\eta = -\frac{q_\mu^2}{4M_N^2}$ and m_π is the pion mass.

B. Exchange currents

As mentioned, we use a phenomenological Lagrangian approach (PhLA) to estimate the contributions of meson-exchange (MEX) currents. In a PhLA due to Ivanov and Truhlik [15], the MEX operators are derived in a hard pion approach [34], in which one explicitly constructs a phenomenological Lagrangian consistent with current algebra, PCAC, and the vector meson dominance. This Lagrangian was used by Tatara *et al.* [6] in their calculations for $\mu - d$ capture and the $\nu - d$ reactions [6]. Meanwhile, the studies by Doi *et al.* [7,21] indicate that only a small subset of the possible diagrams gives essentially the same results as the full set. Based on this experience, we consider here the following types of exchange currents.

Axial-vector current

The axial vector exchange current, A^μ_{MEX}, consists of a pion-pole term and a non-pole part, $\bar{A}^\mu_{MEX}$. Using the PCAC hypothesis, we can express A^μ_{MEX} in terms of the non-pole part alone:

$$A^\mu_{MEX} = \bar{A}^\mu_{MEX} - \frac{q^\mu}{m_\pi^2 - q_\mu^2}(\boldsymbol{q}\cdot\bar{\boldsymbol{A}}_{MEX} - \omega\bar{A}_{MEX,0}). \tag{29}$$

We therefore need only consider the non-pole part. For the time component it is known that one-pion exchange diagram gives the most important contribution, called the KDR current [35]. The explicit form of the KDR current, with a vertex form factor supplemented, reads

$$\begin{aligned}\bar{A}^\pm_{KDR,0}(\boldsymbol{x}) = \frac{1}{if_A}\left(\frac{f}{m_\pi}\right)^2 \delta(\boldsymbol{x}-\boldsymbol{r}_1)[\boldsymbol{\tau}_1\times\boldsymbol{\tau}_2]^{(\pm)} \int \frac{d\boldsymbol{q'}}{(2\pi)^3} K_\pi^2(\boldsymbol{q'}^2)\frac{e^{-i\boldsymbol{q'}\cdot\boldsymbol{r}}}{\omega_\pi^2}(\boldsymbol{\sigma}_2\cdot\boldsymbol{q'}) \\ +(1\leftrightarrow 2),\end{aligned} \tag{30}$$

with $\boldsymbol{r} = \boldsymbol{r}_1 - \boldsymbol{r}_2$ and $\omega_\pi = \sqrt{\boldsymbol{q'}^2 + m_\pi^2}$. For the space component, we take account of the isobar current, $\bar{\boldsymbol{A}}^\pm_\Delta$, that arises from one-pion and one-ρ-meson exchange diagrams. Its explicit form is

$$\bar{\boldsymbol{A}}^{\pm}_{\Delta}(\boldsymbol{x}) = 4\pi f_A \delta(\boldsymbol{x}-\boldsymbol{r}_1)\int \frac{d\boldsymbol{q'}e^{-i\boldsymbol{q'}\cdot\boldsymbol{r}}}{(2\pi)^3}$$
$$\times\left[\frac{K_\pi^2(\boldsymbol{q'}^2)}{\omega_\pi^2}\{c_0\boldsymbol{q'}\boldsymbol{\tau}_2^{(\pm)} + d_1(\boldsymbol{\sigma}_1\times\boldsymbol{q'})[\boldsymbol{\tau}_1\times\boldsymbol{\tau}_2]^{(\pm)}\}(\boldsymbol{\sigma}_2\cdot\boldsymbol{q'})\right.$$
$$\left.+\frac{K_\rho^2(\boldsymbol{q'}^2)}{\omega_\rho^2}\left\{c_\rho\boldsymbol{q'}\times(\boldsymbol{\sigma}_2\times\boldsymbol{q'})\boldsymbol{\tau}_2^{(\pm)} + d_\rho\boldsymbol{\sigma}_1\times(\boldsymbol{q'}\times(\boldsymbol{\sigma}_2\times\boldsymbol{q'}))[\boldsymbol{\tau}_1\times\boldsymbol{\tau}_2]^{(\pm)}\right\}\right]$$
$$+(1\leftrightarrow 2), \tag{31}$$

with $\omega_\rho = \sqrt{\boldsymbol{q'}^2+m_\rho^2}$ and m_ρ is the mass of ρ-meson. For the third component of the isovector current, we just replace $\tau_i^{\pm}$ and $[\boldsymbol{\tau}_1\times\boldsymbol{\tau}_2]^{(\pm)}$ with $\frac{\tau_i^3}{2}$ and $\frac{[\boldsymbol{\tau}_1\times\boldsymbol{\tau}_2]^{(3)}}{2}$, respectively. (This prescription will be applied to other exchange currents as well.) The numerical values of the pion coupling constants can be determined from low-energy pion-nucleon scattering [36], while the ρ-meson coupling constants are deduced from the quark model:

$$\frac{f^2}{4\pi} = 0.08, \quad c_0 m_\pi^3 = 0.188, \quad d_1 m_\pi^3 = -0.044, \quad c_\rho m_\rho^3 = 36.2, \quad d_\rho = -\tfrac{1}{4}c_\rho.$$

Furthermore, we assume that the $\boldsymbol{q}^2$-dependence of the vertex form factors, $K_{mN}(\boldsymbol{q}^2)$ and $K_{m\Delta}(\boldsymbol{q}^2)$ $(m=\pi,\rho)$, are given by $K_{\pi N}(\boldsymbol{q}^2) = K_{\pi\Delta}(\boldsymbol{q}^2) = K_\pi(\boldsymbol{q}^2) = \frac{\Lambda_\pi^2-m_\pi^2}{\Lambda_\pi^2+\boldsymbol{q}^2}$, $K_{\rho N}(\boldsymbol{q}^2) = K_{\rho\Delta}(\boldsymbol{q}^2) = K_\rho(\boldsymbol{q}^2) = \frac{\Lambda_\rho^2-m_\rho^2}{\Lambda_\rho^2+\boldsymbol{q}^2}$, with cutoff masses, $\Lambda_\pi = 1.18$ GeV and $\Lambda_\rho = 1.45$ GeV [37]. We use the above-listed values of coupling constants and form factors as our standard parameters.

Vector current

Regarding the vector exchange currents, we first note that the exchange currents for the time component must be small, since the exchange currents for charge vanish in the static limit. As for the space component, we take into account pair, pionic, and isobar currents. If we adopt the one-pion exchange model for the pair and pionic current and the one-pion and one-ρ-meson exchange model for the isobar current, their explicit forms are given as

$$\boldsymbol{V}^{\pm}_{pair}(\boldsymbol{x}) = -2if_V\left(\frac{f}{m_\pi}\right)^2\delta(\boldsymbol{x}-\boldsymbol{r}_1)[\boldsymbol{\tau}_1\times\boldsymbol{\tau}_2]^{(\pm)}\int\frac{d\boldsymbol{q'}}{(2\pi)^3}K_\pi^2(\boldsymbol{q'}^2)\frac{e^{-i\boldsymbol{q'}\cdot\boldsymbol{r}}}{\omega_\pi^2}\boldsymbol{\sigma}_1(\boldsymbol{\sigma}_2\cdot\boldsymbol{q'})$$
$$+(1\leftrightarrow 2)\,, \tag{32}$$

$$\boldsymbol{V}^{\pm}_{pionic}(\boldsymbol{x}) = 2i\left(\frac{f}{m_\pi}\right)^2 [\boldsymbol{\tau}_1 \times \boldsymbol{\tau}_2]^{(\pm)} \int \frac{d\boldsymbol{q'}_1}{(2\pi)^3} K_\pi(\boldsymbol{q'}^2_1) \int \frac{d\boldsymbol{q'}_2}{(2\pi)^3} K_\pi(\boldsymbol{q'}^2_2)$$
$$\times \frac{e^{-i\boldsymbol{q'}_1\cdot(\boldsymbol{r}_1-\boldsymbol{x})}}{\omega^2_{\pi 1}} \frac{e^{-i\boldsymbol{q'}_2\cdot(\boldsymbol{x}-\boldsymbol{r}_2)}}{\omega^2_{\pi 2}} (\boldsymbol{\sigma}_1\cdot\boldsymbol{q'}_1)(\boldsymbol{\sigma}_2\cdot\boldsymbol{q'}_2)(\boldsymbol{q'}_1+\boldsymbol{q'}_2), \tag{33}$$

$$\boldsymbol{V}^{\pm}_{\Delta}(\boldsymbol{x}) = -\frac{f_V+f_M}{2M_N f_A}\boldsymbol{\nabla}\times\bar{\boldsymbol{A}}^{\pm}_{\Delta}, \tag{34}$$

with $\omega_{\pi i} = \sqrt{m^2_\pi + \boldsymbol{q}'^2_i}$.

C. Nucleon-nucleon potential

In PhLA, the nuclear transition matrix elements are obtained by sandwiching the one-body IA and two-body MEX currents between the initial and final nuclear wave functions which obey the Schrödinger equation that involves a phenomenological nucleon-nucleon potential. The earlier work [6,7] indicates that, so long as we use a realistic NN potential that reproduces with sufficient accuracy the scattering phase shifts and the deuteron properties, the numerical results for the $\nu - d$ cross sections are not too sensitive to particular choices of NN potentials. It seems worthwhile to further check this stability for the *modern* potentials that were not available at the time of the work described in [6,7]. As representatives of the "state-of-the-art" NN potentials, we consider in this work the following three: the Argonne-$v18$ potential (ANLV18) [38], the Reid93 potential [39], and the Nijmegen II potential (NIJ II) [39]. For the sake of definiteness, however, we treat ANLV18 as a primary representative. We shall compare our results with those obtained with the use of the more *traditional* potentials.

D. Monitoring the reliability of the model

Although, as mentioned, there is by now a rather long list of experimental and theoretical work that points to the basic robustness of PhLA calculations, it is desirable to monitor the reliability of our model by simultaneously studying reactions that are closely related to the $\nu - d$ reactions and for which experimental data is available. It turns out that the $\pi N\Delta$

vertex that features in the dominant exchange current for the $\nu - d$ reaction appears also in the $np \to \gamma d$ reaction, for which experimental cross sections are known for a wide range of the incident energy, from the thermal neutron energy up to the pion-production threshold. We therefore calculate here both $\nu - d$ reaction and $np \to \gamma d$ cross sections in the same formalism and use the latter to gauge (at least partially) the reliability of our model.

III. CALCULATIONAL METHODS

A. Multipole expansion of hadron current

To evaluate the two-nucleon matrix element of the hadron current, we first separate the center-of-mass and relative wave functions,

$$< \boldsymbol{r}_1, \boldsymbol{r}_2 \mid d(P) >= e^{i\boldsymbol{P}\cdot\boldsymbol{R}}\psi_d(\boldsymbol{r}), \qquad < \boldsymbol{r}_1, \boldsymbol{r}_2 \mid NN(P') >= e^{i\boldsymbol{P'}\cdot\boldsymbol{R}}\psi_{\boldsymbol{p'}}(\boldsymbol{r}), \tag{35}$$

where $\boldsymbol{r} = \boldsymbol{r}_1 - \boldsymbol{r}_2$ and $\boldsymbol{R} = \frac{\boldsymbol{r}_1+\boldsymbol{r}_2}{2}$, and ψ_d and $\psi_{\boldsymbol{p'}}$ represent, respectively, the deuteron wave function and a scattering-state wave function with asymptotic relative momentum $\boldsymbol{p'}$. Then the matrix element of the hadron current for charged-current reaction is given by

$$j_\lambda^{CC} \equiv< NN(P)' \mid J_\lambda^{CC}(0) \mid d(P) > \; = \int d\boldsymbol{r}\; \psi^*_{\boldsymbol{p'}}(\boldsymbol{r}) \left[\int d\boldsymbol{R}\; e^{-i\boldsymbol{q}\cdot\boldsymbol{R}} J_\lambda^{CC}(0)\right] \psi_d(\boldsymbol{r}). \tag{36}$$

As for the neutral-current reaction, we just replace J_λ^{CC} with J_λ^{NC}. In the following equations, J_λ without superscript applies for both NC and CC. Eliminating the dependence of the current $J_\lambda(\boldsymbol{x})$ on the center-of-mass coordinate, $\boldsymbol{R}$, we can write

$$j_\lambda =< \psi_{p'}| \int d\boldsymbol{x}\; e^{i\boldsymbol{q}\cdot\boldsymbol{x}} \mathcal{J}_\lambda(\boldsymbol{x}) |\psi_d >, \tag{37}$$

where $\mathcal{J}_\lambda(\boldsymbol{x}) \equiv J_\lambda(\boldsymbol{x})|_{\boldsymbol{R}=0}$. Similarly, we define $\mathcal{V}_\lambda(\boldsymbol{x}) \equiv V_\lambda(\boldsymbol{x})|_{\boldsymbol{R}=0}$, and $\mathcal{A}_\lambda(\boldsymbol{x}) \equiv A_\lambda(\boldsymbol{x})|_{\boldsymbol{R}=0}$. We now introduce the standard multipole expansion of the nuclear currents [40]. The multipole operator for the time component of a current is defined by

$$T_C^{JM}(\mathcal{J}) = \int d\boldsymbol{x} j_J(qx) Y_{JM}(\hat{\boldsymbol{x}}) \mathcal{J}_0(\boldsymbol{x}), \tag{38}$$

where $j_J(qx)$ is the spherical Bessel function of order J, $q \equiv |\boldsymbol{q}|$, and $\hat{\boldsymbol{x}} \equiv \boldsymbol{x}/|\boldsymbol{x}|$. The electric and magnetic multipole operators are defined by

$$T_E^{JM}(\mathcal{J}) = \frac{1}{q}\int d\boldsymbol{x}\boldsymbol{\nabla} \times [j_J(qx)\boldsymbol{Y}_{JJM}(\hat{\boldsymbol{x}})] \cdot \boldsymbol{\mathcal{J}}(\boldsymbol{x}), \tag{39}$$

$$T_M^{JM}(\mathcal{J}) = \int d\boldsymbol{x} j_J(qx)\boldsymbol{Y}_{JJM}(\hat{\boldsymbol{x}}) \cdot \boldsymbol{\mathcal{J}}(\boldsymbol{x}), \tag{40}$$

where $\boldsymbol{Y}_{JLM}(\hat{\boldsymbol{x}})$ are vector spherical harmonics. The longitudinal multipole operator is defined by

$$T_L^{JM}(\mathcal{J}) = \frac{i}{q}\int d\boldsymbol{x}\boldsymbol{\nabla}[j_J(qx)Y_{JM}(\hat{\boldsymbol{x}})] \cdot \boldsymbol{\mathcal{J}}(\boldsymbol{x}). \tag{41}$$

Using the conservation of the vector current, the longitudinal multipole operator of the vector current can be related to the charge density operator as

$$T_L^{J_o}(\mathcal{V}) = -\frac{\omega}{q}T_C^{J_o}(\mathcal{V}). \tag{42}$$

An explicit form of the electric multipole operator for the vector current is given by

$$\begin{aligned} T_E^{JM}(\mathcal{V}) = &-i\sqrt{\frac{J}{2J+1}}\int d\boldsymbol{x} j_{J+1}(qx)\boldsymbol{Y}_{JJ+1M}(\hat{\boldsymbol{x}}) \cdot \boldsymbol{\mathcal{V}}(\boldsymbol{x}) \\ &+i\sqrt{\frac{J+1}{2J+1}}\int d\boldsymbol{x} j_{J-1}(qx)\boldsymbol{Y}_{JJ-1M}(\hat{\boldsymbol{x}}) \cdot \boldsymbol{\mathcal{V}}(\boldsymbol{x}). \end{aligned} \tag{43}$$

Here again we can use the current conservation to rewrite Eq.(43) into a form that has the correct long wavelength limit of an electric multipole operator:

$$T_E^{JM}(\mathcal{V}) = -\sqrt{\frac{J+1}{J}}\frac{\omega}{q}T_C^{JM}(\mathcal{V}) - i\sqrt{\frac{2J+1}{J}}\int d\boldsymbol{x} j_{J+1}(qx)\boldsymbol{Y}_{JJ+1M}(\hat{\boldsymbol{x}}) \cdot \boldsymbol{\mathcal{V}}(\boldsymbol{x}). \tag{44}$$

B. Cross sections

As explained earlier, we calculate the cross sections for $\nu/\bar{\nu}(k) + d(P) \to l(k') + N_1(p'_1) + N_2(p'_2)$ in the laboratory system. Following the standard procedure, we obtain the cross section for the CC reaction as

$$d\sigma = \sum_{\bar{i},f} \frac{\delta^4(k + P - k' - P')}{(2\pi)^5}\frac{G_F^2 \cos^2\theta_C}{2} F(Z, E'_\ell)\ |l^\lambda j_\lambda^{CC}|^2 d\boldsymbol{k'} d\boldsymbol{p'}_1 d\boldsymbol{p'}_2, \tag{45}$$

and the cross section for the NC reaction as

$$d\sigma = \sum_{\bar{i},f} \frac{\delta^4(k+P-k'-P')}{(2\pi)^5} \frac{G_F^2}{2} |l^\lambda j_\lambda^{NC}|^2 d\boldsymbol{k'} d\boldsymbol{p'}_1 d\boldsymbol{p'}_2. \tag{46}$$

The matrix elements, l^λ and j_λ, have been defined in Eq.(10) and in Eq.(36), respectively. In Eq.(45), we have included the Fermi function $F(Z, E'_\ell)$ [41] to take into account the Coulomb interaction between the electron and the nucleons. In fact, this factor is relevant only to the $\nu_e + d \to e^- + p + p$ reaction, for which we should use $F(Z=2, E'_\ell)$; for the $\bar{\nu}_e + d \to e^+ + n + n$ reaction we have $F(Z=0, E'_\ell) \equiv 1$.

Substitution of the multipole operators defined in Eq.(38) ∼Eq.(41) leads to

$$\begin{aligned} l^\lambda j_\lambda = & \sum_{J_o M_o} 4\pi i^{J_o} (-1)^{M_o} \\ & \times < \psi_{\boldsymbol{p'}} | \left[T_C^{J_o M_o} \ell_C^{J_o - M_o} + T_E^{J_o M_o} \ell_E^{J_o - M_o} + T_L^{J_o M_o} \ell_L^{J_o - M_o} + T_M^{J_o M_o} \ell_M^{J_o - M_o} \right] | \psi_d >, \end{aligned} \tag{47}$$

where the lepton matrix elements are given as

$$\ell_C^{JM} = Y_{JM}(\hat{\boldsymbol{q}})\ l^0, \tag{48}$$

$$\ell_E^{JM} = \left(\sqrt{\frac{J+1}{2J+1}} \boldsymbol{Y}_{J-1JM}(\hat{\boldsymbol{q}}) + \sqrt{\frac{J}{2J+1}} \boldsymbol{Y}_{J+1JM}(\hat{\boldsymbol{q}}) \right) \cdot \boldsymbol{l}, \tag{49}$$

$$\ell_M^{JM} = \boldsymbol{Y}_{JJM}(\hat{\boldsymbol{q}}) \cdot \boldsymbol{l}, \tag{50}$$

$$\ell_L^{JM} = \left(\sqrt{\frac{J}{2J+1}} \boldsymbol{Y}_{J-1JM}(\hat{\boldsymbol{q}}) - \sqrt{\frac{J+1}{2J+1}} \boldsymbol{Y}_{J+1JM}(\hat{\boldsymbol{q}}) \right) \cdot \boldsymbol{l}. \tag{51}$$

To proceed, we use a scattering wave function of the following form:

$$\begin{aligned} \psi_{\boldsymbol{p'}}(\boldsymbol{r}) = & \sum_{L,S,J,T} 4\pi (1/2, s_1, 1/2, s_2 | S\mu)\ (1/2, \tau_1, 1/2, \tau_2 | T, T_z)\ (LmS\mu | JM) \\ & \times\ i^L Y^*_{L,m}(\hat{\boldsymbol{p}}')\ \psi_{LSJT}(\boldsymbol{r}) \end{aligned} \tag{52}$$

with

$$\psi_{LSJT}(\boldsymbol{r}) = \frac{1-(-1)^{L+S+T}}{\sqrt{2}} \sum_{L'} \mathcal{Y}_{L'SJ}(\hat{\boldsymbol{r}})\ R^J_{L',L;S}(r)\ \eta_{T,T_z}, \tag{53}$$

$$\mathcal{Y}_{LSJ}(\hat{\boldsymbol{r}}) = [Y_L(\hat{\boldsymbol{r}}) \otimes \chi_S]_{(J)}, \tag{54}$$

where χ_S (η_T) is the two-nucleon spin (isospin) wave function with total spin S (isospin T). The above wave function is normalized in such a manner that, in the plane wave limit, it satisfies

$$R^J_{L',L;S}(r) \to j_L(p'r)\delta_{L,L'}. \tag{55}$$

The partial wave expansion of the scattering wave function [Eq.(52)] gives

$$\begin{aligned} l^\lambda j_\lambda = & \sum_{L,S,J,T,m} \sum_{J_o,M_o} (-1)^{M_o}\ i^{J_o-L} \frac{(4\pi)^2}{\sqrt{2J+1}} (1/2, s_1, 1/2, s_2|S\mu)\ (1/2, \tau_1, 1/2, \tau_2|T, T_z) \\ & \times (1 m_d J_o M_o|JM)(LmS\mu|JM)\ Y_{L,m}(\hat{\boldsymbol{p}}') \sum_{X=C,E,L,M} < T^{J_o}_X >\ \ell^{J_o-M_o}_X, \end{aligned} \tag{56}$$

where m_d is the z-component of the deuteron angular momentum. We have used here a simplified notation

$$< O^{J_o} > \ = < \psi_{LSJT} || O^{J_o} || \psi_d > \tag{57}$$

for the reduced matrix element defined by

$$< J'M'|\ O^{J_oM_o}\ |JM> \ = \frac{1}{\sqrt{2J'+1}}\ (J, M, J_o, M_o|J', M') < J'||O^{J_o}||\ J>, \tag{58}$$

where $O^{J_oM_o}$ are the multipole operators that appear in Eq.(38)$\sim$(41).

1. Cross sections for charged-current reaction

For the CC reaction, observables of interest are the total cross section and the lepton differential cross sections. We therefore integrate Eq.(45) over the momenta of the final two nucleons. The evaluation of the phase space integrals and the relevant kinematics are briefly described in the Appendix. According to the Appendix, Eq.(45) leads to

$$d\sigma = \frac{G_F^2 \cos^2\theta_C}{3\pi^2} F(Z, E'_\ell)\, |M|^2 \delta(M_d + k - E'_\ell - P'^0) \bar{J}\, p'^2 dp' k'^2 dk' d\Omega_{\boldsymbol{k}'}, \tag{59}$$

where

$$\begin{aligned} |M|^2 = \sum_{LSJ,J_o} \{ & |< T^{J_o}_C(\mathcal{V}) >|^2 (1 + \hat{\boldsymbol{k}}\cdot\boldsymbol{\beta} + \frac{\omega^2}{\boldsymbol{q}^2}\ (1 - \hat{\boldsymbol{k}}\cdot\boldsymbol{\beta} + 2\ \hat{\boldsymbol{q}}\cdot\boldsymbol{\beta}\ \hat{\boldsymbol{q}}\cdot\hat{\boldsymbol{k}}) - \frac{2\omega}{q}\ \hat{\boldsymbol{q}}\cdot(\hat{\boldsymbol{k}} + \boldsymbol{\beta})) \\ & + |< T^{J_o}_C(\mathcal{A}) >|^2 (1 + \hat{\boldsymbol{k}}\cdot\boldsymbol{\beta}) + |< T^{J_o}_L(\mathcal{A}) >|^2 (1 - \hat{\boldsymbol{k}}\cdot\boldsymbol{\beta} + 2\ \hat{\boldsymbol{q}}\cdot\boldsymbol{\beta}\ \hat{\boldsymbol{q}}\cdot\hat{\boldsymbol{k}}) \\ & + 2Re[< T^{J_o}_C(\mathcal{A}) >< T^{J_o}_L(\mathcal{A}) >^*]\ \hat{\boldsymbol{q}}\cdot(\hat{\boldsymbol{k}} + \boldsymbol{\beta}) \\ & + [|< T^{J_o}_M(\mathcal{V}) >|^2 + |< T^{J_o}_E(\mathcal{V}) >|^2 + |< T^{J_o}_M(\mathcal{A}) >|^2 + |< T^{J_o}_E(\mathcal{A}) >|^2]\ (1 - \hat{\boldsymbol{q}}\cdot\hat{\boldsymbol{k}}\ \hat{\boldsymbol{q}}\cdot\boldsymbol{\beta}) \\ & \mp 2Re[< T^{J_o}_M(\mathcal{V}) >< T^{J_o}_E(\mathcal{A}) >^* + < T^{J_o}_M(\mathcal{A}) >< T^{J_o}_E(\mathcal{V}) >^*]\ \hat{\boldsymbol{q}}\cdot(\hat{\boldsymbol{k}} - \boldsymbol{\beta})\ \}\,. \end{aligned} \tag{60}$$

In the above, $k' \equiv |\boldsymbol{k}'|$ and $\boldsymbol{\beta} \equiv \boldsymbol{k}'/E'_\ell$; $\boldsymbol{p}'$ is the relative momentum of the final two nucleons, and $p' \equiv |\boldsymbol{p}'|$. Of the double sign in the last line of Eq.(60), the upper (lower) sign corresponds to the ν ($\bar{\nu}$) reaction. The appearance of the factor $\bar{J}$ in Eq.(59) needs an explanation. As discussed in the Appendix, when relativistic kinematics is adopted, there arises a Jacobian, J, associated with the introduction of $\boldsymbol{p}'$ but it is a good approximation to use $\bar{J}$, the angle-averaged value of J.

For the total cross section, the use of relativistic kinematics gives

$$\sigma = \int dT \int d(\cos\theta_L) \frac{G_F^2 \cos^2\theta_C}{3\pi} \frac{\bar{J} E'_\ell \left(\sqrt{P'^2_\mu}/2\right) p' k'}{1 + E'_\ell (1 - k\cos\theta_L/k')/\sqrt{P'^2_\mu + \boldsymbol{q}^2}} F(Z, E'_\ell) |M|^2, \qquad (61)$$

where T is the kinetic energy of the final NN relative motion and θ_L is the lepton scattering angle $\cos\theta_L = \hat{\boldsymbol{k}} \cdot \hat{\boldsymbol{k}'}$ in the laboratory frame. If instead we use non-relativistic kinematics, the results would be

$$\sigma = \int dT \int d(\cos\theta_L) \frac{G_F^2 \cos^2\theta_C}{3\pi} \frac{E'_\ell (2M_r) p' k'}{1 + E'_\ell (1 - k\cos\theta_L/k')/(M_{N1} + M_{N2})} F(Z, E'_\ell) |M|^2, \quad (62)$$

where M_{Ni} is the mass of the i-th nucleon, and M_r is the reduced mass of the final NN system.

Eq.(59) also leads to the double differential cross sections for the $\nu_e + d \to e^- + p + p$ reaction:

$$\frac{d^2\sigma}{d\Omega_{\boldsymbol{k}'} dE'_\ell} = \frac{G_F^2 \cos^2\theta_C}{12\pi^2} F(Z, E'_\ell) \bar{J} p' k' E'_\ell \sqrt{P'^2_\mu + \boldsymbol{q}^2}\ |M|^2. \qquad (63)$$

The electron energy spectrum and the electron angular distribution are obtained from Eq.(63) as

$$\frac{d\sigma}{dE'_\ell} = \int d\Omega_{\boldsymbol{k}'} \left(\frac{d^2\sigma}{d\Omega_{\boldsymbol{k}'} dE'_\ell}\right)_{\text{Eq.(63)}} \qquad \frac{d\sigma}{d\Omega_{\boldsymbol{k}'}} = \int dE'_\ell \left(\frac{d^2\sigma}{d\Omega_{\boldsymbol{k}'} dE'_\ell}\right)_{\text{Eq.(63)}}. \qquad (64)$$

2. Cross sections for neutral-current reaction

The total cross section for the NC reaction can be calculated in essentially the same manner as above. The result is

$$\sigma = \int dT \int d(\cos\theta_L) \frac{2G_F^2}{3\pi} \frac{\bar{J} E'_\ell \left(\sqrt{P'^2_\mu}/2\right) p' k'}{1 + E'_\ell (1 - k\cos\theta_L/k')/\sqrt{P'^2_\mu + \boldsymbol{q}^2}} |M|^2 \,, \tag{65}$$

where $|M|^2$ is given by Eq.(60) with, however, the charged current replaced by the neutral current. By contrast, in calculating neutron differential cross sections we can no longer integrate over the relative momentum of the final nucleons. We therefore work with the following expressions:

$$\frac{d^2\sigma}{d\Omega_{\boldsymbol{p}'_n} dT_n} = \int d\Omega_{\boldsymbol{k}'} \frac{G_F^2}{3(2\pi)^5} \frac{E_p k'^2 p'_n E_n}{E_p - \boldsymbol{p}'_p \cdot \hat{\boldsymbol{k}}'} \sum_{m_d, s_n, s_p} |j_\lambda l^\lambda|^2, \tag{66}$$

where we have indicated explicitly averaging over the initial spin and summing over the final spins. The energy and momentum of the final proton (neutron) are denoted by $(E'_\alpha, \boldsymbol{p'}_\alpha)$ with $\alpha = p$ ($\alpha = n$); T_n is the kinetic energy of the neutron. The neutron energy spectrum and the neutron angular distribution are then evaluated as

$$\frac{d\sigma}{dT_n} = \int d\Omega_{\boldsymbol{p}'_n} \left(\frac{d^2\sigma}{d\Omega_{\boldsymbol{p}'_n} dT_n}\right)_{\text{Eq.(66)}} \qquad \frac{d\sigma}{d\Omega_{\boldsymbol{p}'_n}} = \int dT_n \left(\frac{d^2\sigma}{d\Omega_{\boldsymbol{p}'_n} dT_n}\right)_{\text{Eq.(66)}} . \tag{67}$$

The calculation of the total cross section for the $np \to \gamma d$ reaction follows essentially the same pattern as that of the $\nu - d$ total cross section, and therefore we forgo its description.

IV. NUMERICAL RESULTS

A. Radiative capture of neutron on proton

To test the nuclear currents and wave functions used, we first discuss the capture rate for $np \to \gamma d$. Thermal neutron capture is a well known case for testing exchange currents [17,18]. This reaction is dominated by the isovector magnetic dipole transition from the $^1S_0$ np scattering state. With the use of the ANLV18 potential, our PhLA calculation gives $\sigma(np \to \gamma d) = 335.1$ mb, with both the IA and MEX currents included. This is in good agreement with the experimental value, $\sigma(np \to \gamma d)^{exp} = 334.2 \pm 0.5$ mb [42]. With the IA contribution alone, our result would be $\sigma(np \to \gamma d)^{IA} = 304.5$ mb. The 10% contribution of the exchange current is due to the pion, pair and Δ-currents.

Going beyond the thermal neutron energy regime, we give in Fig.1 the calculated $\sigma(np \to \gamma d)$ as a function of the incident neutron kinetic energy, T_n. The experimental data in Fig.1 have been obtained from either the neutron capture reaction itself [43] or its inverse process [44,45], using detailed balance for the latter. We can see that our results describe very well the energy dependence of $\sigma(np \to \gamma d)^{exp}$ all the way up to $T_n \approx 100$ MeV. The figure indicates that the electric dipole amplitude starts to become important around T_n=100 keV. In the higher energy region we should expect deviations from the long-wave length limit of the electric dipole operator, and therefore the good agreement of our results with the data suggests that the description of the electric multipole is also satisfactory.[6] The fact that our PhLA calculation with no *ad hoc* adjustment of the input parameters is capable of reproducing $\sigma(np \to \gamma d)^{exp}$ for a very wide range of the incident energy gives us a reasonable degree of confidence in the basic idea of PhLA and the input parameters used.[7] Of course, strictly speaking, the electromagnetic and weak-interaction processes do not probe exactly the same sectors of PhLA, but the remarkable success with $\sigma(np \to \gamma d)$ gives, at least, partial justification of our PhLA as applied to weak-interaction reactions. Noting that the dominant axial MEX current due to Δ-excitation is related to the Δ-excitation MEX current for the vector current (we need only replace $(f_V + f_M)/2M_N$ with f_A), we evaluate the former with the same input parameters as used in calculating $\sigma(np \to \gamma d)$.

B. Cross sections of $\nu - d$ reactions

We now present our numerical results for the $\nu(\bar{\nu}) - d$ reactions. In what follows, the *"standard run"* represents our full calculation with the following features. The ANLV18 potential [38] is used to generate the initial and final two-nucleon states and the final two-

---

[6]Since our treatment here does not include pion production, our results should be taken with caution above the pion production threshold.

[7]Another similar success of PhLA is known in the $d(e, e')np$ reaction [18].

nucleon partial waves are included up to $J = 6$. For the transition operators, we use the IA and MEX operators described in Sec. II; the Siegert theorem is invoked for the electric part of the vector current. As regards the single-nucleon weak-interaction form factors, we employ the most updated parameterization given in Eqs.(22)-(28). The final two-nucleon system is treated relativistically in the sense explained in Appendix.[8] Our numerical results will be given primarily for our *standard run*; other cases are presented mostly in the context of examining the model dependence.

1. Total cross sections for $\nu - d$ and $\bar{\nu} - d$ reactions

We give in TABLE I and Fig.2 the total cross sections, obtained in our *standard run*, for the four reactions: $\nu_e d \to e^- pp,\ \nu_x d \to \nu_x np,\ \bar{\nu}_e d \to e^+ nn,\ \bar{\nu}_x d \to \bar{\nu}_x np$. The cross sections are given as functions of E_ν, the incident $\nu/\bar{\nu}$ energy, from the threshold to $E_\nu = 170$ MeV. [9] It should be mentioned that towards the highest end of E_ν considered here, pion production sets in but the present calculation does not include it.

It is informative to decompose the total cross section into partial-wave contributions. TABLE II shows the relative importance of the two lowest partial waves in the final two-nucleon state; denoting the contributions to the total cross section from the $^1S_0$ and ^3P_J states by $\sigma(^1S_0)$ and $\sum_J \sigma(^3P_J)$, respectively, we give in TABLE II the ratios, $\sigma(^1S_0)/\sigma(\text{all})$ and $\sum_{J=0}^{2} \sigma(^3P_J)/\sigma(\text{all})$, as functions of E_ν. Here $\sigma(\text{all})$ denotes the sum of the contributions of all the partial waves; in fact, it is sufficient to include up to $J = 6$ even for $E_\nu = 170$ MeV, where the summed contribution of higher partial waves ($J > 6$) is found to be less than 1%. The table reconfirms that, in the low-energy region, the Gamow-Teller (GT) amplitude

---

[8] We must emphasize that our calculation takes account of "relativity" only in certain aspects of kinematics. Going beyond this is out of the scope of this paper.

[9] The numerical results reported in this article are available in tabular and graphical forms at the web site: <http://nuc003.psc.sc.edu/~kubodera/NU-D-NSGK>.

due to the ${}^1S_0$ final state gives a dominant contribution. It is therefore important to take into account the Δ-excitation axial-vector current, which gives a main correction to the IA current. As mentioned, in our approach, the coupling constant determining the Δ-excitation MEX current is controlled by the $np \to \gamma d$ amplitude. As E_ν increases, the ${}^3P_J$ final states become as important as the ${}^1S_0$ state, and therefore 1^- type multipole operators arising from the vector as well as axial-vector currents start to play a significant role. In this sense it is reassuring that the validity of our model for the electric dipole matrix element in this energy region has been tested in the photo-reaction.

Turning now to TABLE III, we give in the second column labeled "IA", the ratio of the total cross section obtained with the use of the IA terms alone to that of our *standard run*. We see that, at the low energies, the MEX contribution is about 5% of the IA contribution. As E_ν increases, the relative importance of the MEX current contribution augments and it can reach as much as 8% in the high energy region. We also have found that the Siegert theorem allows us to take into account implicitly most part of the MEX for the vector current. At high energies, whether or not one implements the Siegert theorem leads to 1% difference. The MEX for the axial-charge is found to be very small for the entire energy range considered here.

In order to compare our cross sections with those of the previous work, we give in TABLE III the ratios of the cross sections reported in YHH [8] and in KN [10] to those of our *standard run*; the third column gives $\sigma(\mathrm{YHH})/\sigma(\mathit{standard\ run})$, while the fourth column shows $\sigma(\mathrm{KN})/\sigma(\mathit{standard\ run})$. In the solar neutrino energy region, one can see that the results of our *standard run* agree with those of KN [10] within 1% except for the $\nu_e d \to e^- pp$ reaction near threshold, wherein the discrepancy can reach 2%. As the incident energy becomes higher, our results start to be somewhat larger than those of KN, and the difference becomes about 6% towards the higher end of E_ν. This variance arises largely

from the cutoff mass in the form factor $G_A(q^2)$, which accounts for 3-4% difference.[10] The remaining ∼2% difference is due to our use of relativistic kinematics and the inclusion of the contributions from higher partial waves and from the isoscalar current which were ignored in the previous study. We have done an additional calculation by running our code adopting the same approximations and the same input parameters as in KN, and confirmed that the results agree with those of KN within 1%.[11]

On the other hand, the cross sections of YHH [8] are about 5% smaller than those of our *standard run* even at the low energy. This reflects the fact that YHH did not include the MEX contributions (except for the term that could be incorporated via the extended Siegert theorem). Indeed, comparison of the YHH cross sections with the entries in the second column labeled "IA" in TABLE III indicates that, if we drop the explicit MEX terms in our calculation, the resulting cross sections in the solar energy region agree with those of YHH within ∼1%.

We next consider the NN-potential dependence of the cross sections. The fifth column labeled "Reid93" in TABLE III gives the ratio of the total cross section obtained with the use of the Reid93 potential [39] to that of our *standard run*; the sixth column gives a similar ratio for the case of the NIJ II potential [39]. We note that the dependence on the nuclear potentials is within 1% for all the reactions and for the entire energy region under study. [12]

---

[10]The value of m_A in [33] was deduced from an experiment involving a deuteron target and therefore it may involve nuclear effects. It seems worthwhile to reanalyze the data taking into account possible nuclear effects. Another potentially useful source of information on m_A is low-energy pion electroproduction [46].

[11]The precision of our numerical computation of the cross sections is also 1%.

[12]There is 2% variance for the $\bar{\nu}_e d \to e^+ nn$ cross section near threshold (not shown here); this is however very likely to be attributable to the fact that the n-n scattering length is not exactly reproduced by the potentials other than ANLV18.

Since all the potentials used here describe the NN scattering data to a satisfactory degree, it is probably not extremely surprising that all these *modern* realistic NN potentials give essentially identical results for $\nu - d$ cross sections, but the present explicit confirmation is reassuring.

In our calculation the strength of the Δ-excitation exchange current, which contributes both to the Gamow-Teller and M1 transitions, is monitored by the empirical values for $\sigma(np \to \gamma d)$. Meanwhile, Carlson *et al.* [22], in estimating the solar *pp*-fusion cross section, used the tritium β-decay rate to fine-tune the $\pi N\Delta$ coupling constant that features in the Gamow-Teller exchange current. This method turns out to yield somewhat "quenched" Δ-excitation MEX effects in the *pp* fusion. It is therefore of interest to study the consequences of this second method for the $\nu - d$ reactions. In the last column labeled "Δ(CRSW)" of TABLE III, we give the ratio of the cross sections obtained with the use of the Δ-current employed in [22] to those of our *standard run*. In the solar energy region this ratio is found to be 0.96 - 0.97, or the MEX contribution relative to the IA term is 2%, instead of 5% found in our *standard run*. This reduction is primarily due to the smaller $\pi N\Delta$ coupling constant in [22]. At higher neutrino energies, the use of the the Δ-current employed in [22] leads to a $\sim$4% MEX effect relative to the IA term, to be compared with the $\sim$8% effect found in our *standard run*. Thus, in general, if we adopt the approach taken in [22], the importance of the MEX effect relative to the IA contribution will be reduced by a factor of $\sim$2 as compared with the result of our *standard run*.

As emphasized by Bahcall *et al.* [31], one of the crucial quantities in neutrino oscillation studies at the SNO is the double ratio [NC]/[CC], where [NC] ([CC]) itself is the ratio of the observed neutrino absorption rate to the standard theoretical estimate for the NC (CC) reaction rate. This implies that the reliability of theoretical estimates for the ratio $R \equiv \sigma(NC)/\sigma(CC) \equiv \sigma(\nu d \to \nu np)/\sigma(\nu_e d \to e^- pp)$ is extremely important. We give in Table IV the values of R resulting from the various models considered in this paper. Since our primary interest here is to examine the model dependence of R, we choose, in Table IV, to normalize R by $R_{standard\,run}$, the value corresponding to our *standard run*; $R_{standard\,run}$

itself is shown in the second column of the table. We learn from Table IV that all the models studied give essentially the same R; deviations from $R_{standard\,run}$ are at most $\sim$1%. Thus, the largest source of model dependence in our work due to the Δ-exchange current cancels out by taking the ratio between the NC and CC reactions.

2. Differential cross sections for the electron

We now discuss three types of electron differential cross sections for the $\nu_e + d \to e^- + p + p$ reaction: (i) the energy spectrum, $d\sigma/dE'_e$ in Eq.(64), (ii) the electron angular distribution, $d\sigma/d\Omega_{\boldsymbol{k}'}$ in Eq.(64), and (iii) the electron double differential cross sections, $d^2\sigma/dE'_e d\Omega_{\boldsymbol{k}'}$ in Eq.(63). Although this kind of information must be implicitly contained in the computer codes used in the existing work [6–10], its explicit tabulation has been lacking in the literature. It seems very useful to make these differential cross sections readily available to our research community. However, a trivial but nonetheless serious problem is that the required amount of tabulation is enormous. We therefore present here some representative results, relegating the bulk of tabulation to a web site.[13] For four values of the incident neutrino energies, E_ν = 5, 10, 20 and 150 MeV, we give the electron-energy spectra, $d\sigma/dE'_e$, in Fig.3 and the electron angular distribution, $d\sigma/d\Omega_{\boldsymbol{k}'}$, in Fig.4. We note that the electron spectrum in Fig.3 exhibits a "cusp-like" structure for E_ν=150 MeV. This feature, which is in fact common for $E_\nu \geq 100$ MeV, probably calls for an explanation. For a given value of E_ν, we can separate the electron energy E'_e into two ranges: $E'_e < E'^c_e$ or $E'_e > E'^c_e$, where E'^c_e is the point above which the electron scattering angle θ_L cannot any longer cover the full range $[0, \pi]$ for a kinematic reason.[14] The "cusp-like" structure occurs at $E'_e = E'^c_e$ due to interplay between the change in the range in the phase space integral and the momentum dependence in the transition matrix element for the final $^1S_0$ channel. This structure, however, is *not*

---

[13] See footnote 9.

[14] See the Appendix.

a cusp in the mathematical sense. Enlarging the scale of the abscissa, we can confirm that the actual curve is a rapidly changing but non-singular one. It turns out that for higher values of E_ν we need more scale enlargement before the curve starts looking smooth to the eye. This is the reason why, for a fixed abscissa scale (as adopted in our illustration), the case corresponding to the high incident energy tends to exhibit more "cusp-like" behavior.

Regarding the electron angular distribution (Fig.4), we note that at low neutrino energies the electrons are emitted in the backward direction, carrying most of the available energy. The angular distributions for the lower incident energies are reminiscent of that for a Gamow-Teller β-decay between two bound states. If we simplify the expression for the electron differential cross section, (Eq.(63)), by dropping all the partial waves other than $^1S_0$ and by retaining only the leading-order Gamow-Teller matrix element, then we have

$$d\sigma \sim \frac{G_F^2 \cos^2\theta_C}{12\pi^3} f_A^2 M_p p' k'^2 F(Z, E'_e)\ (3 - \beta\cos\theta_L) I^2 dk' d\Omega_{\boldsymbol{k'}}, \tag{68}$$

where I is the relevant radial integral. Since $\beta \sim 1$ and $F \sim 1$, if we tentatively treat I as a constant, we have a simple expression

$$d\sigma \propto p' k'^2\ (3 - \cos\theta_L) dk' d\Omega_{\boldsymbol{k'}}. \tag{69}$$

In fact, the electron angular distributions for low incident neutrino energies can be simulated to high accuracy by Eq.(69); see the dotted lines in Fig.4. Thus, although the radial integral I may in fact depend strongly on the kinetic energy of the NN relative motion, the numerical results for $d\sigma/d\Omega_{\boldsymbol{k'}}$ at the low energies can be conveniently simulated by the simple phase-space formula, Eq.(69).

As for the electron double differential cross sections, $d^2\sigma/dE'_e d\Omega_{\boldsymbol{k'}}$, Eq.(63), even presenting some typical cases is impractical because of the bulkiness of the tables. We therefore relegate their tabulation completely to the web site the address of which is given in footnote 9.

Finally, we consider the neutron energy spectrum, $d\sigma/dT_n$ and the neutron angular distribution, $d\sigma/d\Omega_n$ in Eq.(67), for the $\nu + d \to \nu + p + n$ reaction. For $E_\nu = 5, 10, 20$, and 50 MeV, we show $d\sigma/dT_n$ in Fig.5 and $d\sigma/d\Omega_n$ in Fig.6. Once again, we relegate a complete tabulation of our numerical results to the web site mentioned in footnote 9. We see from Figs.5 and 6 that the neutron energy spectrum has a peak near the lower end, and that, unlike the electrons, the neutrons are emitted in the forward direction.

V. DISCUSSION AND SUMMARY

Based on a phenomenological Lagrangian approach (PhLA), we have carried out a detailed study of the $\nu - d$ reactions and provided the total cross sections and the differential cross sections for the electrons and neutrons, from threshold to $E_\nu = 170$ MeV. We have examined the influence of changes in various inputs that feature in our PhLA. In particular, we have studied to what extent the use of the modern NN potentials affects the results. We have also examined the influence of the use of the updated input concerning the nucleon weak-interaction form factors. The vertex strength that governs the Δ-excitation axial-vector exchange current has been monitored using the photo-reaction. We have also studied the consequence of employing the vertex strength determined with the use of the tritium β-decay strength [22].

For the solar energy region, $E_\nu < 20$ MeV, the results are summarized as follows. By comparing our new results with those in the literature, we have confirmed that the total $\nu - d$ cross sections are stable within 1% precision against any changes in the input that have been studied, except for somewhat higher sensitivity to the strength of the Δ-current (see below). The same stability should also exist for the differential cross sections described in this paper. The MEX axial-vector current increases the total cross sections by $\sim$5% from the IA values, and it is extremely unlikely that this 5% increase is completely in error, for we have used

the $np \to \gamma d$ reaction to monitor the dominant part of the MEX current. Meanwhile, Carlson *et al.* [22], in estimating the solar *pp*-fusion cross section, used the tritium β-decay lifetime to monitor a vertex strength that features in the Gamow-Teller exchange current. The results of [22] indicates that adjusting the MEX strength using the tritium β-decay rate could lead to a somewhat reduced MEX amplitude. If we use the Δ-excitation axial current renormalized by the tritium β-decay [22], the MEX current correction to the IA term, $[\sigma(\mathrm{IA}+\mathrm{MEX})-\sigma(\mathrm{IA})]/\sigma(\mathrm{IA})$, turns out to be $\sim$2%, instead of 5% as in our *standard run*; see the column labeled Δ(CRSW) in TABLE III. The difference between our *standard run* and Δ(CRSW) represents the range of uncertainty in the present PhLA calculation. Thus we believe it reasonable to use, as the best estimates of the low-energy νd cross sections, the values given by our *standard run* and attach to them a possible *overall* reduction factor κ, with κ ranging from 0.97 to 1. We propose to adopt this error estimate in lieu of using the entire difference between the cross sections given in YHH [8] and KN [10]. We have shown that in the ratio $R \equiv \sigma(\mathrm{NC})/\sigma(\mathrm{CC})$ the model dependence is reduced down to the 1% level (see TABLE IV).

At higher incident neutrino energies, the results obtained in our *standard run* are somewhat larger than those of KN, and the difference reaches $\sim$6% towards E_ν=150 MeV. This difference is caused largely by the updated value for the axial-vector mass. The effect of relativistic kinematics, as discussed here, has $\sim$1% effect on the cross sections. The contributions of the isoscalar current, which so far has been totally ignored in the literature, is found to be of 1% even at $E_\nu \simeq 150$ MeV. The importance of the MEX currents relative to the IA contributions increases monotonically as E_ν augments. Towards E_ν=150 MeV, the MEX to IA ratio, $[\sigma(\mathrm{IA}+\mathrm{MEX})-\sigma(\mathrm{IA})]/\sigma(\mathrm{IA})$, reaches $\sim$8% in our *standard run* while this ratio is $\sim$4% in the case of Δ(CRSW).

As mentioned earlier in the text, the numerical results of this work are fully documented in tabular or graphical form at the website referred to in footnote 9. It is hoped that those tables and graphs are of value for the ongoing and future neutrino experiments that involve deuteron targets.

ACKNOWLEDGEMENTS

The authors wish to express their sincere thanks to John Bahcall and Arthur McDonald for their interest in the present work. KK is deeply indebted to Malcolm Butler and Jiunn-Wei Chen for the enlightening communication on Refs. [11,12]. TS would like to gratefully acknowledge the hospitality extended to him at the USC Nuclear Physics Group, where the present collaboration started. This work is supported in part by the Ministry of Education, Science, Sport and Culture, Grant-in-Aid for Scientific Research on Priority Areas (A)(2) 12047233, and by the National Science Foundation, USA, Grant No. PHY-9900756.

APPENDIX A: PHASE SPACE INTEGRAL AND KINEMATICS

We briefly explain the derivation of the cross section formula Eq.(59) starting from Eq.(45). The phase space integral in Eq.(59) is

$$\begin{aligned} I &= \delta^4(k + P - k' - P')\ d\boldsymbol{p'}_1 d\boldsymbol{p'}_2 d\boldsymbol{k'} \\ &= \delta(E_\nu + M_d - E'_\ell - \sqrt{\boldsymbol{P'}^2 + P'^2_\mu}\ )\ d\boldsymbol{p'}_L d\boldsymbol{k'}, \end{aligned} \tag{A1}$$

where $\boldsymbol{p'}_L = (\boldsymbol{p'}_1 - \boldsymbol{p'}_2)/2$ and $\boldsymbol{P'} = \boldsymbol{q} = \boldsymbol{k} - \boldsymbol{k'}$.

The scattering energy of the final NN distorted wave is given by their center-of-mass energy $W_{NN} = \sqrt{P^2_\mu}$. The relative momentum in the center-of-mass system, p'^μ, is given by Lorenz-transforming the relative momentum in the lab system as [47]

$$p'^\mu = \Lambda^\mu_\nu\ p'^\nu_L. \tag{A2}$$

The magnitude of $\boldsymbol{p'}$ is related to W_{NN} as

$$W_{NN} = \sqrt{p'^2 + M^2_{N1}} + \sqrt{p'^2 + M^2_{N2}}, \tag{A3}$$

where M_{Ni} is the mass of the i-th nucleon in the final state. The integral over the momentum $\boldsymbol{p'}_L$ is then replaced by integration over $\boldsymbol{p'}$, which gives rise to a Jacobian [47],

$$d\boldsymbol{p'}_L = J d\boldsymbol{p'}, \tag{A4}$$

with

$$J = \frac{4E_1' E_2'}{W_{NN}(E_1' + E_2')}, \tag{A5}$$

where E_i' is the energy of the i-th nucleon in the lab system. Although J depends on the direction of $\boldsymbol{p'}$, we approximate it by $\bar{J} = \frac{1}{4\pi}\int J d\Omega_{\boldsymbol{p'}}$; through a plane-wave calculation, we have confirmed that this is a good approximation in the energy region of our concern. The phase space integral is then given as

$$I = \delta(E_\nu + M_d - E_\ell' - \sqrt{\boldsymbol{P'}^2 + P_\mu'^2}\ )\ \bar{J} d\boldsymbol{p'} d\boldsymbol{k'}, \tag{A6}$$

which leads to Eq.(59).

The kinematically allowed domain of the integral $d\boldsymbol{p'}d\boldsymbol{k'}$ is determined by a standard procedure. We give here the results for the electron energy spectrum, Eq.(64), for the $\nu_e + d \to e^- + p + p$ reaction. The threshold neutrino energy E_ν^{th} for this reaction is given by

$$E_\nu^{th} = \frac{(2M_p + M_d + m_e)(2M_p - M_d + m_e)}{2M_d}. \tag{A7}$$

We may specify the allowed region of the electron energy E_e' by giving the conditions on the electron momentum k'; these conditions are

$$\begin{cases} 0 \le k' \le k_+' & \text{for} \quad E_\nu \ge E_\nu^c \\ k_-' \le k' \le k_+' & \text{for} \quad E_\nu^c \ge E_\nu \ge E_\nu^{th}, \end{cases} \tag{A8}$$

where

$$E_\nu^c \equiv \frac{(2M_p + M_d - m_e)(2M_p - M_d + m_e)}{2(M_d - m_e)}, \tag{A9}$$

and

$$k_\pm' = \frac{E_\nu X \pm (E_\nu + M_d)\sqrt{X^2 - 4m_e^2 W^2}}{2W^2}, \tag{A10}$$

with $W^2 = (P + k)_\mu^2$ and $X \equiv M_d^2 + 2E_\nu M_d - 4M_p^2 + m_e^2$. For given values of E_ν and E_e', the electron scattering angle θ_L is restricted as

$$\max\left\{-1, \frac{2E'_e(M_d+E_\nu)-X}{2E_\nu k'}\right\} \leq \cos\theta_L \leq 1, \tag{A11}$$

and the NN scattering energy is specified by p' given as

$$p' = \frac{1}{2}\sqrt{X + 2E_\nu k' \cos\theta_L - 2E'_e(M_d+E_\nu)}. \tag{A12}$$

For $E_\nu = 150$ MeV, the allowed ranges of $\cos\theta_L$ and p' are plotted as functions of E'_e in Fig.7 and Fig.8, respectively; the dotted area in each figure represents the allowed region. At $E'_e = E'^c_e$, the constraint on θ_L sets in and the minimum value of p' becomes zero. E'^c_e is determined from the condition:

$$2E'^c_e(M_d+E_\nu) + 2E_\nu k'^c - X = 0. \tag{A13}$$

REFERENCES

[1] S. D. Ellis and J. N. Bahcall, Nucl. Phys. **A114**, 636 (1968).

[2] F. T. Avignone III, Phys. Rev. D **24**, 778 (1981).

[3] S. Nozawa, Y. Kohyama, T. Kaneta and K. Kubodera, J. Phys. Soc. Jpn. **55**, 2636 (1986).

[4] J. N. Bahcall, K. Kubodera and S. Nozawa, Phys. Rev. D **38**, 1030 (1988).

[5] S. Ying, W. C. Haxton and E. M. Henley, Phys. Rev. D **40**, 3211 (1989).

[6] N. Tatara, Y. Kohyama and K. Kubodera, Phys. Rev. C **42**, 1694 (1990).

[7] M. Doi and K. Kubodera, Phys. Rev. C **45**, 1988 (1992).

[8] S. Ying, W. C. Haxton and E. M. Henley, Phys. Rev. C **45**, 1982 (1992).

[9] Y. Kohyama and K. Kubodera, USC(NT)-Report-92-1 (1992) (unpublished); M. Doi and K. Kubodera (unpublished).

[10] K. Kubodera and S. Nozawa, Int. J. Mod. Phys. E **3**, 101 (1994).

[11] M. Butler and J.-W. Chen, Nucl. Phys. **A675**, 575 (2000); nucl-th/9905059.

[12] M. Butler, J.-W. Chen and X. Kong, nucl-th/0008032.

[13] The SNO Collaboration, Phys. Lett. **B194**, 321 (1987); nucl-ex/9910016; G. T. Ewan *et al.*, Sudbury Neutrino Observatory Proposal SNO-87-12, 1987.

[14] M. Chemtob and M. Rho, Nucl. Phys. **A163**, 1 (1971).

[15] E. Ivanov and E. Truhlik, Nucl. Phys. **A316**, 451 (1979); **A316**, 437 (1979).

[16] I. S. Towner, Phys. Rep. **155**, 263 (1987).

[17] D. O. Riska and G. E. Brown, Phys. Lett. **38B**, 193 (1972).

[18] See e.g., B. Frois and J.-F. Mathiot, Com. Part. Nucl. Phys. **18**, 291 (1989), and refer-

ences therein.

[19] T. Sato, T. Niwa and H. Ohtsubo, in *Proceedings of the IV International Symposium on Weak and Electromagnetic Interactions in Nuclei*, edited by H. Ejiri, T. Kishimoto and T. Sato (World Scientific, Singapore, 1995), p. 488.

[20] F. Dautry, M. Rho and D. O. Riska, Nucl. Phys. **A264**, 507 (1976).

[21] M. Doi, T. Sato, H. Ohtsubo and M. Morita, Nucl. Phys. **A511**, 507 (1990).

[22] J. Carlson, D. O. Riska, R. Schiavilla and R. B. Wiringa, Phys. Rev. C **44**, 619 (1991).

[23] S. E. Willis *et al.*, Phys. Rev. Lett. **44**, 522 (1980).

[24] S. P. Riley, Z. D. Greenwood, W. R. Kropp, L. R. Price, F. Reines, H. W. Sobel, Y. Declais, A. Etenko and M. Skorokhvatov, Phys. Rev. C **59**, 1780 (1999).

[25] T.-S. Park, D.-P. Min and M. Rho, Phys. Rev. Lett. **74**, 4153 (1995); Nucl. Phys. **A596**, 515 (1996).

[26] T.-S. Park, K. Kubodera, D.-P. Min and M. Rho, Phys. Rev. C **58**, 637 (1998); Astrophys. J. **507**, 443 (1998); Nucl. Phys. **A646**, 83 (1999); Phys. Lett. **B472**, 232 (2000).

[27] U. van Kolck, Prog. Part. Nucl. Phys. **43**, 337 (1999), and references therein.

[28] D. B. Kaplan, M. J. Savage and M. B. Wise, Nucl. Phys. **B478**, 629 (1996); Phys. Lett. **B424**, 390 (1998); Nucl. Phys. **B534**, 329 (1998); Phys. Rev. C **59**, 617 (1999).

[29] J.-W. Chen, H. W. Greißhammer, M. J. Savage and R. P. Springer, Nucl. Phys. **A644**, 221 (1998); **A644**, 245 (1998); D. B. Kaplan, M. J. Savage, R. P. Springer and M. B. Wise, Phys. Lett. **B449**, 1 (1999); T. Mehen and I. W. Stewart, Phys. Lett. **B445**, 378 (1999); X. Kong and F. Ravndal, Phys. Lett. **B450**, 320 (1999).

[30] D. R. Phillips and T. D. Cohen, nucl-th/9906091, and references therein.

[31] J. N. Bahcall, P. I. Krastev and A. Yu. Smirnov, hep-ph/0002293.

[32] M. Gourdin, Phys. Rep. **11**, 29 (1974).

[33] T. Kitagaki *et al.*, Phys. Rev. D **42**, 1331 (1990).

[34] V. I. Ogievetsky and B. M. Zupnik, Nucl. Phys. **B24**, 612 (1970).

[35] K. Kubodera, J. Delorme, and M. Rho, Phys. Rev. Lett. **40**, 755 (1978).

[36] S. L. Adler, Ann. Phys. **50**, 189 (1968); P. Guichon, M. Giffon, J. Joseph, R. Laverrière and C. Samour, Z. Phys. A **285**, 183 (1978).

[37] J. W. Durso, A. D. Jackson and B. J. Verwest, Nucl. Phys. **A282**, 404 (1977); F. Iachello, A. D. Jackson and A. Lande, Phys. Lett. **43B**, 191 (1973).

[38] R. B. Wiringa, V. G. J. Stoks and R. Schiavilla, Phys. Rev. C **51**, 38 (1995).

[39] V. G. J. Stoks, R. A. M. Klomp, C. P. F. Terheggen, and J. J. de Swart, Phys. Rev. C **49**, 2950 (1994).

[40] J. D. Walecka, in *Muon Physics*, edited by V. W. Hughes and C. S. Wu (Academic, New York, 1975), Vol. 2, p. 113.

[41] See e.g., M. Morita, *Beta Decay and Muon Capture*, (W. A. Benjamin, Inc., 1973) p. 27.

[42] A. E. Cox, S. A. R. Wynchank and C. H. Collie, Nucl. Phys. **74**, 497 (1965).

[43] T. S. Suzuki, Y. Nagai, T. Shima, T. Kikuchi, H. Sato, T. Kii and M. Igashira, Astrophys. J. **439**, 59 (1995).

[44] Y. Birenbaum, S. Kahane and R. Moreh, Phys. Rev. C **32**, 1825 (1985).

[45] R. Bernabei *et al.*, Phys. Rev. Lett. **57**, 1542 (1986).

[46] A. Liesenfeld *et al.*, Phys. Lett. **B468**, 20 (1999).

[47] W. Glöckle and Y. Nogami, Phys. Rev. D **35**, 3840 (1987).

TABLES

TABLE I. Total cross sections for $\nu - d$ reactions in units of cm^2. The "$-x$" in parentheses denotes 10^{-x}; thus an entry like 4.279 (-47) stands for 4.279 $\times 10^{-47}$ cm^2.

E_ν [MeV]	$\nu\ d \to \nu\ p\ n$	$\bar{\nu}\ d \to \bar{\nu}\ p\ n$	$\nu_e\ d \to e^-\ p\ p$	$\bar{\nu}_e\ d \to e^+\ n\ n$
2.0	0.000 (0)	0.000 (0)	3.603 (-45)	0.000 (0)
2.2	0.000 (0)	0.000 (0)	7.833 (-45)	0.000 (0)
2.4	4.279 (-47)	4.248 (-47)	1.404 (-44)	0.000 (0)
2.6	4.258 (-46)	4.222 (-46)	2.242 (-44)	0.000 (0)
2.8	1.457 (-45)	1.443 (-45)	3.315 (-44)	0.000 (0)
3.0	3.355 (-45)	3.320 (-45)	4.639 (-44)	0.000 (0)
3.2	6.286 (-45)	6.213 (-45)	6.228 (-44)	0.000 (0)
3.4	1.038 (-44)	1.025 (-44)	8.095 (-44)	0.000 (0)
3.6	1.574 (-44)	1.553 (-44)	1.025 (-43)	0.000 (0)
3.8	2.246 (-44)	2.213 (-44)	1.271 (-43)	0.000 (0)
4.0	3.060 (-44)	3.012 (-44)	1.547 (-43)	0.000 (0)
4.2	4.024 (-44)	3.956 (-44)	1.855 (-43)	1.115 (-45)
4.4	5.142 (-44)	5.049 (-44)	2.196 (-43)	4.554 (-45)
4.6	6.420 (-44)	6.297 (-44)	2.570 (-43)	1.010 (-44)
4.8	7.860 (-44)	7.702 (-44)	2.978 (-43)	1.787 (-44)
5.0	9.468 (-44)	9.267 (-44)	3.420 (-43)	2.799 (-44)
5.2	1.125 (-43)	1.100 (-43)	3.897 (-43)	4.059 (-44)
5.4	1.320 (-43)	1.289 (-43)	4.410 (-43)	5.578 (-44)
5.6	1.533 (-43)	1.495 (-43)	4.959 (-43)	7.364 (-44)
5.8	1.763 (-43)	1.718 (-43)	5.544 (-43)	9.427 (-44)
6.0	2.012 (-43)	1.958 (-43)	6.166 (-43)	1.177 (-43)
6.2	2.279 (-43)	2.215 (-43)	6.825 (-43)	1.441 (-43)
6.4	2.564 (-43)	2.490 (-43)	7.522 (-43)	1.733 (-43)
6.6	2.868 (-43)	2.782 (-43)	8.258 (-43)	2.056 (-43)
6.8	3.191 (-43)	3.092 (-43)	9.031 (-43)	2.409 (-43)
7.0	3.532 (-43)	3.419 (-43)	9.843 (-43)	2.792 (-43)
7.2	3.893 (-43)	3.764 (-43)	1.069 (-42)	3.206 (-43)
7.4	4.273 (-43)	4.126 (-43)	1.159 (-42)	3.652 (-43)
7.6	4.672 (-43)	4.506 (-43)	1.252 (-42)	4.127 (-43)
7.8	5.091 (-43)	4.904 (-43)	1.349 (-42)	4.635 (-43)
8.0	5.529 (-43)	5.320 (-43)	1.450 (-42)	5.175 (-43)
8.2	5.987 (-43)	5.754 (-43)	1.555 (-42)	5.746 (-43)
8.4	6.464 (-43)	6.206 (-43)	1.664 (-42)	6.349 (-43)
8.6	6.961 (-43)	6.676 (-43)	1.777 (-42)	6.984 (-43)
8.8	7.479 (-43)	7.163 (-43)	1.894 (-42)	7.652 (-43)
9.0	8.016 (-43)	7.669 (-43)	2.016 (-42)	8.351 (-43)
9.2	8.573 (-43)	8.193 (-43)	2.141 (-42)	9.082 (-43)
9.4	9.150 (-43)	8.735 (-43)	2.271 (-42)	9.846 (-43)

TABLE I. (continued) Total cross sections for $\nu - d$ reactions in units of cm^2. The "$-x$" in parentheses denotes 10^{-x}; thus an entry like 4.279 (-47) stands for 4.279 $\times 10^{-47}$ cm^2.

E_ν [MeV]	$\nu\ d \to \nu\ p\ n$	$\bar{\nu}\ d \to \bar{\nu}\ p\ n$	$\nu_e\ d \to e^-\ p\ p$	$\bar{\nu}_e\ d \to e^+\ n\ n$
9.6	9.747 (-43)	9.294 (-43)	2.405 (-42)	1.064 (-42)
9.8	1.036 (-42)	9.872 (-43)	2.544 (-42)	1.147 (-42)
10.0	1.100 (-42)	1.047 (-42)	2.686 (-42)	1.233 (-42)
10.2	1.166 (-42)	1.108 (-42)	2.833 (-42)	1.322 (-42)
10.4	1.234 (-42)	1.171 (-42)	2.984 (-42)	1.415 (-42)
10.6	1.304 (-42)	1.236 (-42)	3.139 (-42)	1.510 (-42)
10.8	1.376 (-42)	1.303 (-42)	3.299 (-42)	1.609 (-42)
11.0	1.450 (-42)	1.372 (-42)	3.463 (-42)	1.712 (-42)
11.2	1.526 (-42)	1.442 (-42)	3.631 (-42)	1.817 (-42)
11.4	1.604 (-42)	1.514 (-42)	3.804 (-42)	1.925 (-42)
11.6	1.684 (-42)	1.588 (-42)	3.981 (-42)	2.037 (-42)
11.8	1.767 (-42)	1.664 (-42)	4.163 (-42)	2.152 (-42)
12.0	1.851 (-42)	1.741 (-42)	4.349 (-42)	2.270 (-42)
12.2	1.938 (-42)	1.821 (-42)	4.539 (-42)	2.392 (-42)
12.4	2.026 (-42)	1.902 (-42)	4.734 (-42)	2.516 (-42)
12.6	2.117 (-42)	1.985 (-42)	4.933 (-42)	2.644 (-42)
12.8	2.210 (-42)	2.069 (-42)	5.137 (-42)	2.775 (-42)
13.0	2.305 (-42)	2.156 (-42)	5.346 (-42)	2.909 (-42)
13.5	2.551 (-42)	2.379 (-42)	5.887 (-42)	3.258 (-42)
14.0	2.811 (-42)	2.614 (-42)	6.456 (-42)	3.626 (-42)
14.5	3.084 (-42)	2.860 (-42)	7.054 (-42)	4.015 (-42)
15.0	3.371 (-42)	3.117 (-42)	7.681 (-42)	4.422 (-42)
15.5	3.671 (-42)	3.385 (-42)	8.338 (-42)	4.849 (-42)
16.0	3.984 (-42)	3.663 (-42)	9.024 (-42)	5.295 (-42)
16.5	4.311 (-42)	3.953 (-42)	9.740 (-42)	5.760 (-42)
17.0	4.651 (-42)	4.253 (-42)	1.049 (-41)	6.244 (-42)
17.5	5.006 (-42)	4.564 (-42)	1.126 (-41)	6.747 (-42)
18.0	5.374 (-42)	4.886 (-42)	1.207 (-41)	7.268 (-42)
18.5	5.755 (-42)	5.218 (-42)	1.291 (-41)	7.809 (-42)
19.0	6.151 (-42)	5.561 (-42)	1.378 (-41)	8.367 (-42)
19.5	6.560 (-42)	5.915 (-42)	1.468 (-41)	8.944 (-42)
20.0	6.984 (-42)	6.279 (-42)	1.561 (-41)	9.539 (-42)
20.5	7.421 (-42)	6.653 (-42)	1.657 (-41)	1.015 (-41)
21.0	7.872 (-42)	7.038 (-42)	1.757 (-41)	1.078 (-41)
21.5	8.338 (-42)	7.434 (-42)	1.859 (-41)	1.143 (-41)
22.0	8.817 (-42)	7.839 (-42)	1.965 (-41)	1.210 (-41)
22.5	9.311 (-42)	8.255 (-42)	2.074 (-41)	1.278 (-41)
23.0	9.819 (-42)	8.681 (-42)	2.187 (-41)	1.348 (-41)
23.5	1.034 (-41)	9.117 (-42)	2.303 (-41)	1.420 (-41)
24.0	1.088 (-41)	9.564 (-42)	2.422 (-41)	1.494 (-41)
24.5	1.143 (-41)	1.002 (-41)	2.545 (-41)	1.569 (-41)

TABLE I. (continued) Total cross sections for $\nu - d$ reactions in units of cm^2. The "$-x$" in parentheses denotes 10^{-x}; thus an entry like 4.279 (-47) stands for 4.279 $\times 10^{-47}$ cm^2.

E_ν [MeV]	$\nu\ d \to \nu\ p\ n$	$\bar{\nu}\ d \to \bar{\nu}\ p\ n$	$\nu_e\ d \to e^-\ p\ p$	$\bar{\nu}_e\ d \to e^+\ n\ n$
25	1.199 (-41)	1.049 (-41)	2.671 (-41)	1.646 (-41)
26	1.317 (-41)	1.145 (-41)	2.933 (-41)	1.805 (-41)
27	1.440 (-41)	1.245 (-41)	3.209 (-41)	1.971 (-41)
28	1.569 (-41)	1.350 (-41)	3.499 (-41)	2.143 (-41)
29	1.704 (-41)	1.458 (-41)	3.803 (-41)	2.322 (-41)
30	1.845 (-41)	1.570 (-41)	4.121 (-41)	2.507 (-41)
31	1.992 (-41)	1.685 (-41)	4.454 (-41)	2.698 (-41)
32	2.145 (-41)	1.805 (-41)	4.802 (-41)	2.896 (-41)
33	2.304 (-41)	1.928 (-41)	5.164 (-41)	3.099 (-41)
34	2.469 (-41)	2.055 (-41)	5.541 (-41)	3.309 (-41)
35	2.640 (-41)	2.186 (-41)	5.934 (-41)	3.525 (-41)
36	2.817 (-41)	2.320 (-41)	6.342 (-41)	3.746 (-41)
37	3.001 (-41)	2.458 (-41)	6.765 (-41)	3.973 (-41)
38	3.190 (-41)	2.600 (-41)	7.204 (-41)	4.206 (-41)
39	3.386 (-41)	2.745 (-41)	7.659 (-41)	4.445 (-41)
40	3.588 (-41)	2.893 (-41)	8.130 (-41)	4.689 (-41)
41	3.796 (-41)	3.045 (-41)	8.617 (-41)	4.938 (-41)
42	4.011 (-41)	3.200 (-41)	9.120 (-41)	5.193 (-41)
43	4.232 (-41)	3.359 (-41)	9.639 (-41)	5.453 (-41)
44	4.459 (-41)	3.521 (-41)	1.018 (-40)	5.718 (-41)
45	4.692 (-41)	3.686 (-41)	1.073 (-40)	5.988 (-41)
46	4.932 (-41)	3.854 (-41)	1.130 (-40)	6.264 (-41)
47	5.178 (-41)	4.026 (-41)	1.188 (-40)	6.544 (-41)
48	5.430 (-41)	4.201 (-41)	1.248 (-40)	6.829 (-41)
49	5.689 (-41)	4.379 (-41)	1.310 (-40)	7.119 (-41)
50	5.954 (-41)	4.559 (-41)	1.374 (-40)	7.413 (-41)
51	6.226 (-41)	4.743 (-41)	1.440 (-40)	7.712 (-41)
52	6.504 (-41)	4.930 (-41)	1.507 (-40)	8.016 (-41)
53	6.788 (-41)	5.120 (-41)	1.575 (-40)	8.324 (-41)
54	7.079 (-41)	5.313 (-41)	1.646 (-40)	8.636 (-41)
55	7.376 (-41)	5.509 (-41)	1.718 (-40)	8.953 (-41)
60	8.957 (-41)	6.528 (-41)	2.107 (-40)	1.060 (-40)
65	1.070 (-40)	7.612 (-41)	2.540 (-40)	1.233 (-40)
70	1.260 (-40)	8.757 (-41)	3.018 (-40)	1.415 (-40)
75	1.465 (-40)	9.959 (-41)	3.540 (-40)	1.606 (-40)
80	1.686 (-40)	1.121 (-40)	4.108 (-40)	1.802 (-40)
85	1.922 (-40)	1.250 (-40)	4.721 (-40)	2.004 (-40)
90	2.172 (-40)	1.383 (-40)	5.378 (-40)	2.212 (-40)
95	2.437 (-40)	1.520 (-40)	6.079 (-40)	2.424 (-40)
100	2.715 (-40)	1.660 (-40)	6.824 (-40)	2.640 (-40)
105	3.007 (-40)	1.803 (-40)	7.612 (-40)	2.859 (-40)

TABLE I. (continued) Total cross sections for $\nu - d$ reactions in units of cm^2. The "$-x$" in parentheses denotes 10^{-x}; thus an entry like 4.279 (-47) stands for 4.279 $\times 10^{-47}$ cm^2.

E_ν [MeV]	$\nu\ d \to \nu\ p\ n$	$\bar{\nu}\ d \to \bar{\nu}\ p\ n$	$\nu_e\ d \to e^-\ p\ p$	$\bar{\nu}_e\ d \to e^+\ n\ n$
110	3.313 (-40)	1.949 (-40)	8.440 (-40)	3.081 (-40)
115	3.630 (-40)	2.097 (-40)	9.307 (-40)	3.306 (-40)
120	3.958 (-40)	2.247 (-40)	1.021 (-39)	3.532 (-40)
125	4.298 (-40)	2.397 (-40)	1.116 (-39)	3.760 (-40)
130	4.648 (-40)	2.549 (-40)	1.214 (-39)	3.990 (-40)
135	5.009 (-40)	2.702 (-40)	1.315 (-39)	4.220 (-40)
140	5.378 (-40)	2.855 (-40)	1.420 (-39)	4.452 (-40)
145	5.756 (-40)	3.009 (-40)	1.528 (-39)	4.684 (-40)
150	6.143 (-40)	3.163 (-40)	1.639 (-39)	4.918 (-40)
155	6.539 (-40)	3.318 (-40)	1.753 (-39)	5.151 (-40)
160	6.941 (-40)	3.472 (-40)	1.870 (-39)	5.385 (-40)
165	7.350 (-40)	3.627 (-40)	1.989 (-39)	5.621 (-40)
170	7.765 (-40)	3.781 (-40)	2.111 (-39)	5.856 (-40)

TABLE II. Contributions of the two lowest partial waves. For several representative values of the incident neutrino energy E_ν are shown the ratios, $\sigma(^1S_0)/\sigma(\text{all})$ and $\sum_{J=0}^{2}\sigma(^3P_J)/\sigma(\text{all})$, as defined in the text.

	$d(\nu,\nu)pn$		$d(\nu,e^-)pp$	
E_ν[MeV]	$^1S_0$	^3P_J	$^1S_0$	^3P_J
5	0.999	0.001	0.999	0.001
10	0.995	0.005	0.993	0.007
20	0.972	0.027	0.964	0.035
50	0.827	0.158	0.804	0.182
100	0.589	0.334	0.561	0.366
150	0.433	0.410	0.409	0.442

TABLE III. Model dependence of total cross sections. The second column (IA) gives the ratio of the results of the IA calculation to those of the *standard run*. The third column (YHH) and the fourth column (KN) give σ(YHH)/σ(*standard run*) and σ(KN)/σ(*standard run*), respectively. The fifth column (Reid93) [sixth column (NIJ II)] gives the ratio of the total cross section obtained with the use of the Reid 93 potential [Nijmegen II potential] to that of our *standard run*. The last column (Δ(CRSW)) gives the ratio of the total cross section obtained with the Δ-current of Carlson *et al.* to that of our *standard run*.

$d(\nu,\nu)pn$						
E_ν[MeV]	IA	YHH	KN	Reid93	NIJ II	Δ(CRSW)
5	0.949	0.962	1.002	0.997	1.002	0.965
10	0.942	0.955	1.003	0.998	1.002	0.961
20	0.934	0.946	1.000	0.998	1.001	0.956
50	0.927	0.964	0.993	0.999	1.000	0.953
100	0.925	0.961	0.971	1.000	1.000	0.953
150	0.924	0.915	0.943	1.000	0.999	0.954
$d(\nu,e^-)pp$						
E_ν[MeV]	IA	YHH	KN	Reid93	NIJ II	Δ(CRSW)
5	0.952	0.956	1.019	1.003	1.003	0.968
10	0.945	0.949	1.008	1.003	1.002	0.964
20	0.937	0.948	1.002	1.002	1.001	0.959
50	0.928	0.961	0.990	1.001	1.000	0.956
100	0.924	0.955	0.968	1.001	0.999	0.956
150	0.922	0.897	0.941	1.001	0.999	0.956

TABLE IV. Model dependence of $R \equiv \sigma(NC)/\sigma(CC) \equiv \sigma(\nu d \to \nu np)/\sigma(\nu_e d \to e^- pp)$. For representative values of E_ν, R for our *standard run* is given in the second column. The third through the sixth columns give R_a, with a = IA, Reid93, NIJ II, and Δ(CRSW), normalized by $R_{standard\ run}$. See also the caption for TABLE III.

E_ν[MeV]	$R_{standard\ run}$	IA	Reid93	NIJ II	Δ(CRSW)
5	0.277	0.997	0.994	0.999	0.997
10	0.410	0.997	0.996	1.000	0.997
20	0.447	0.997	0.997	1.000	0.997
50	0.433	0.999	0.998	1.000	0.997
100	0.398	1.001	0.999	1.000	0.997
150	0.375	1.003	1.000	1.001	0.998

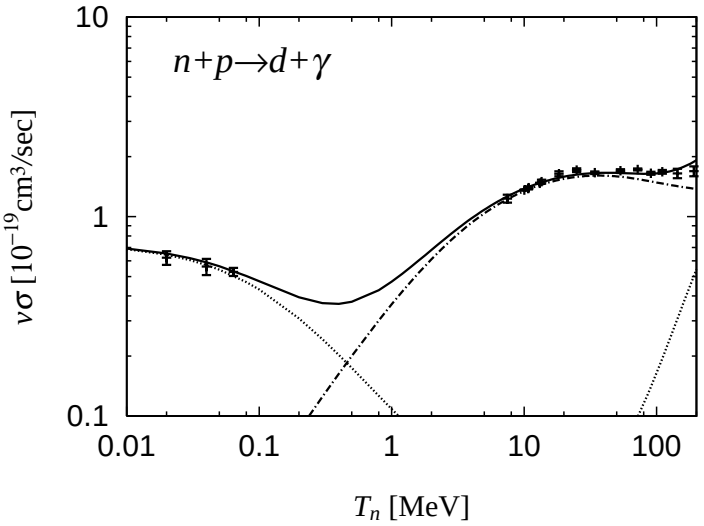

FIG. 1. Total cross section for radiative neutron capture. The solid curve corresponds to the results of our full calculation including the IA and exchange currents and all the multipole amplitudes. The dashed and dash-dotted curves show the individual contributions of the magnetic-dipole and electric-dipole amplitudes, respectively. The data are taken either from the neutron capture reaction itself [43], or from its inverse process [44,45], with the use of detailed balance for the latter.

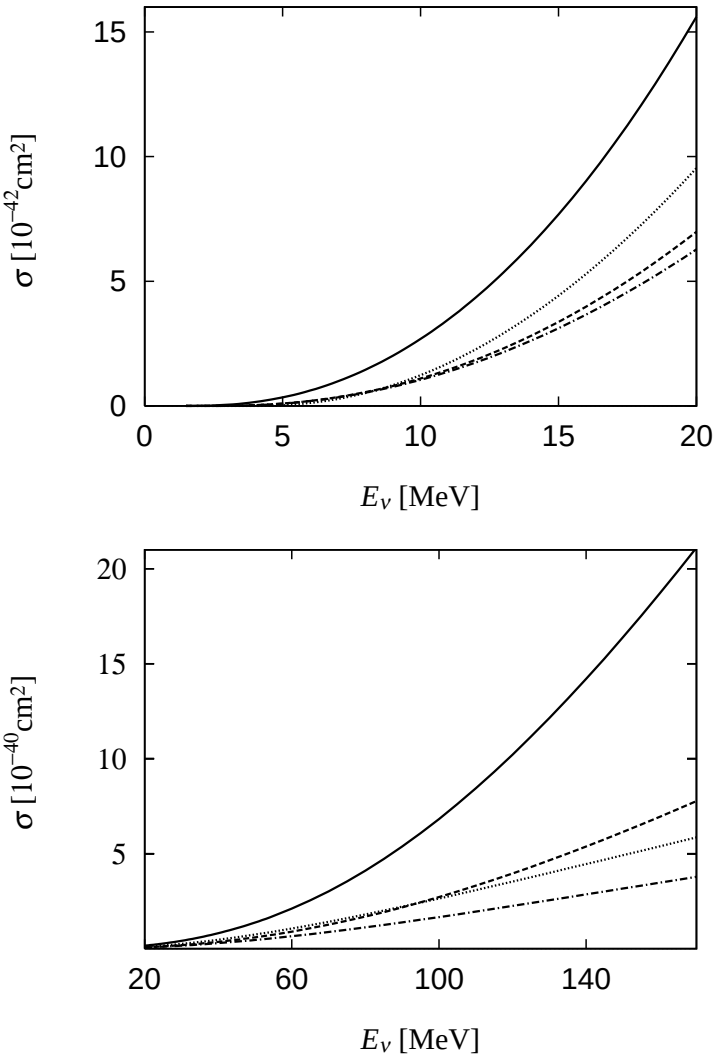

FIG. 2. Total cross section for the reactions: $\nu_e d \to e^- pp$, $\bar{\nu}_e d \to e^+ nn$, $\nu d \to \nu pn$, and $\bar{\nu} d \to \bar{\nu} pn$. The solid and dotted curves show the charged-current reaction cross sections for ν and $\bar{\nu}$, respectively, while the long-dash and dash-dotted curves give the neutral-current reaction cross sections for ν and $\bar{\nu}$, respectively.

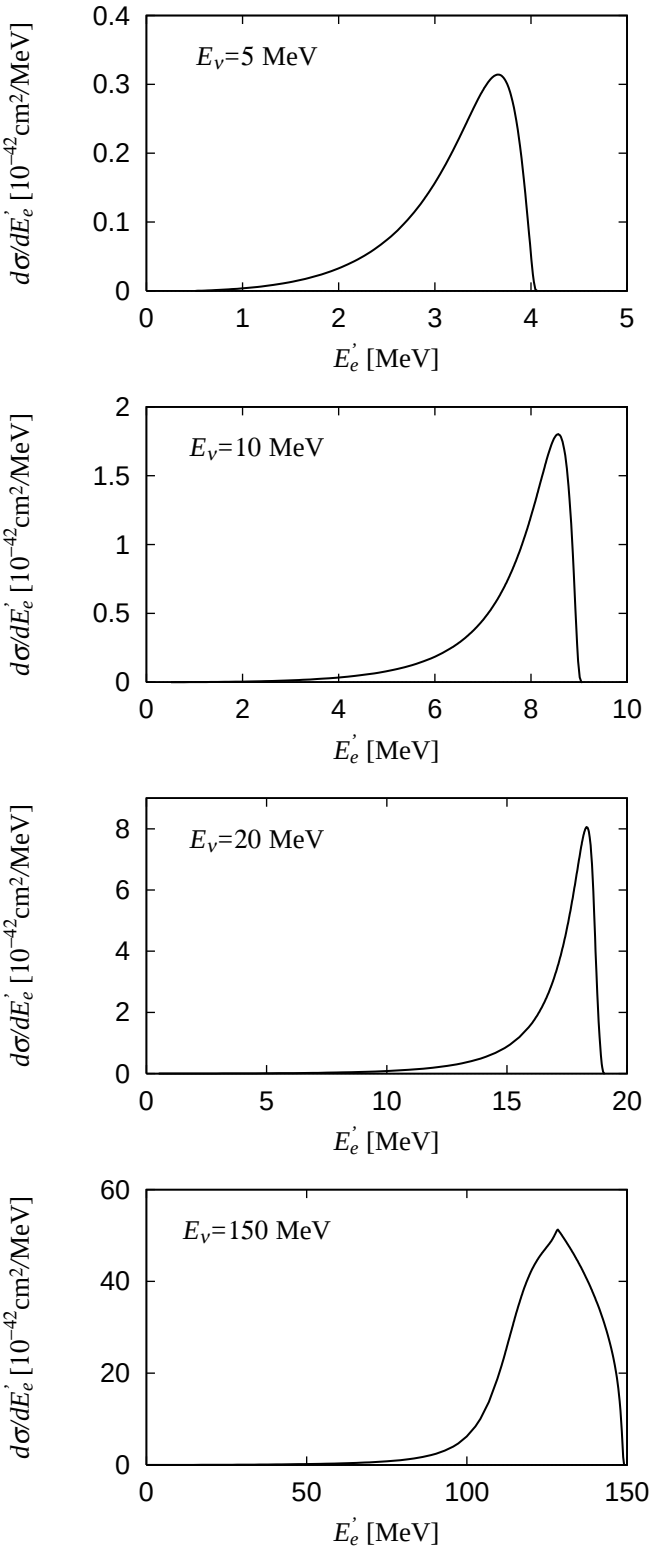

FIG. 3. Electron energy spectra for the $\nu_e d \to e^- pp$ reaction.

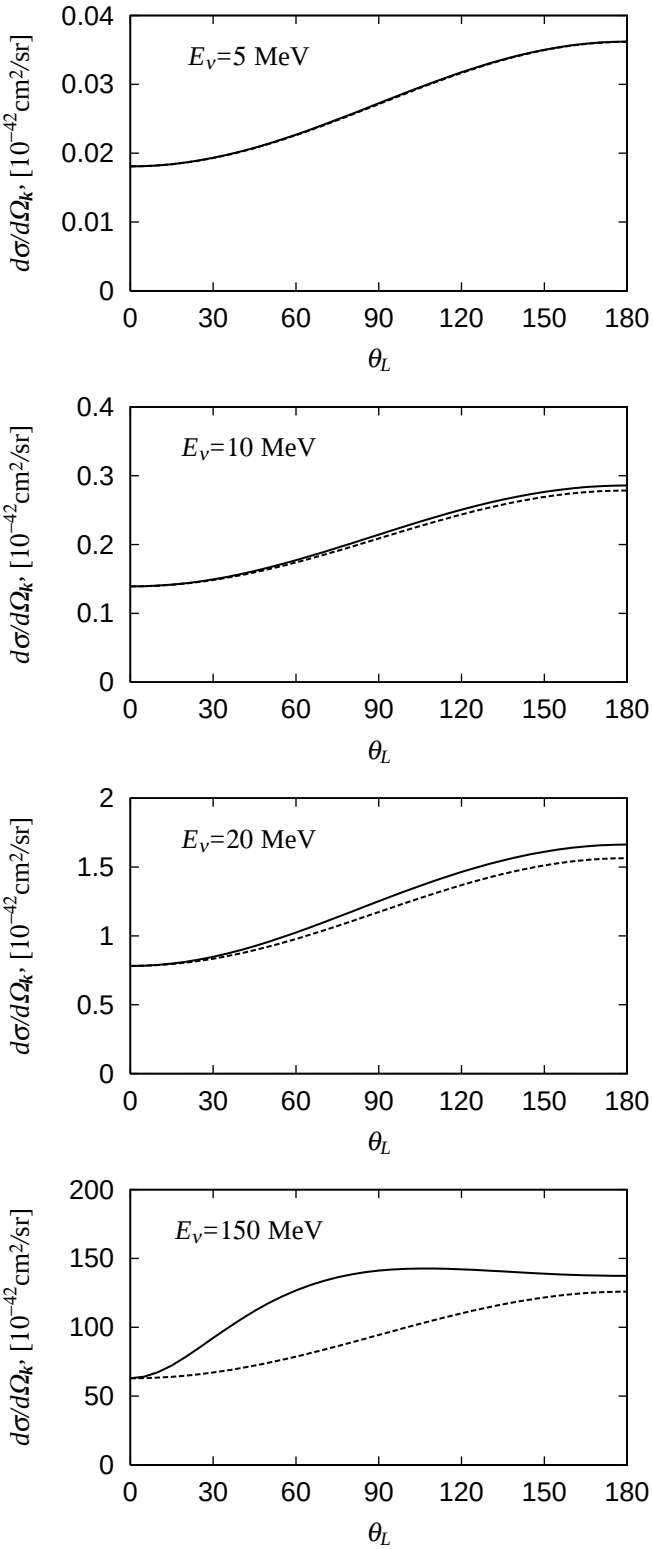

FIG. 4. Electron angular distribution for the $\nu_e d \to e^- pp$ reaction. The solid curves show the results of our *standard run*, while the dotted curves correspond to the simplified expression, Eq.(69), normalized to the *standard run* results at $\theta_L = 0$.

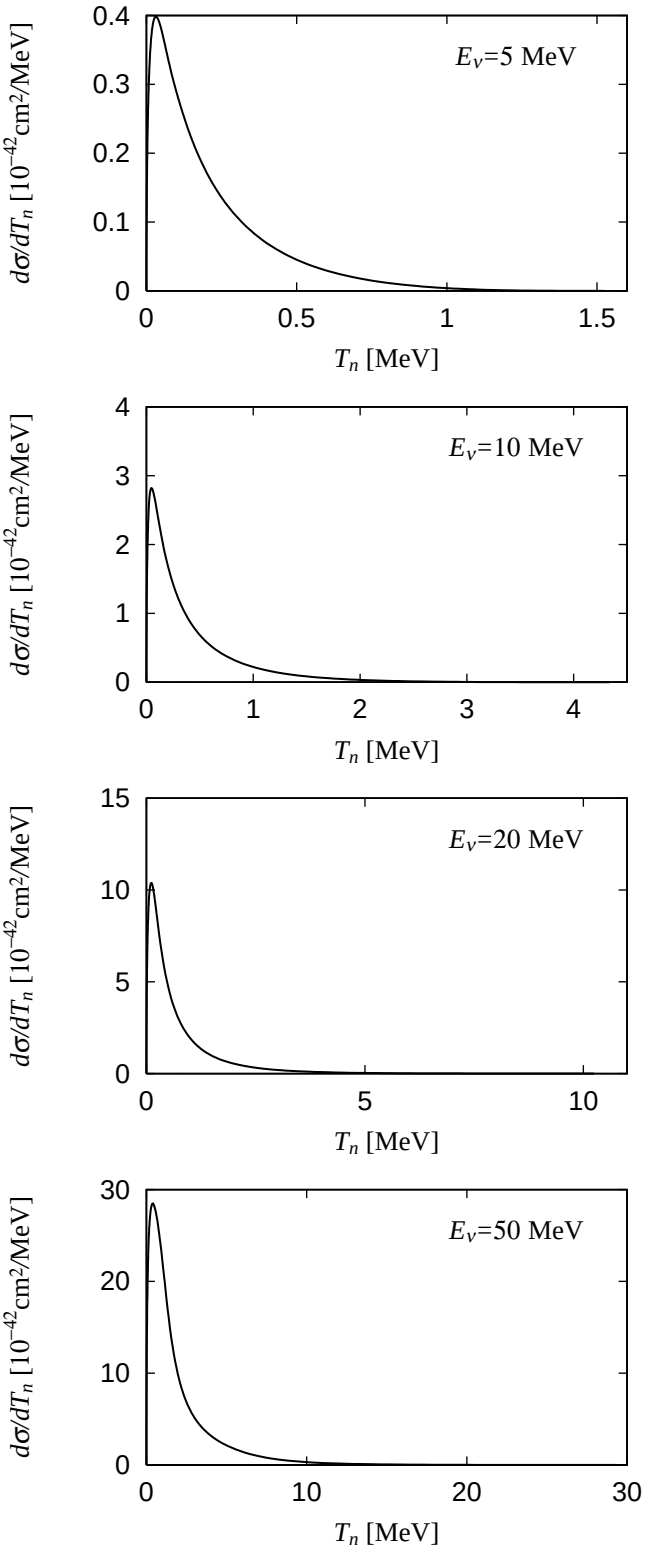

FIG. 5. Neutron energy spectra for the $\nu d \to \nu pn$ reaction.

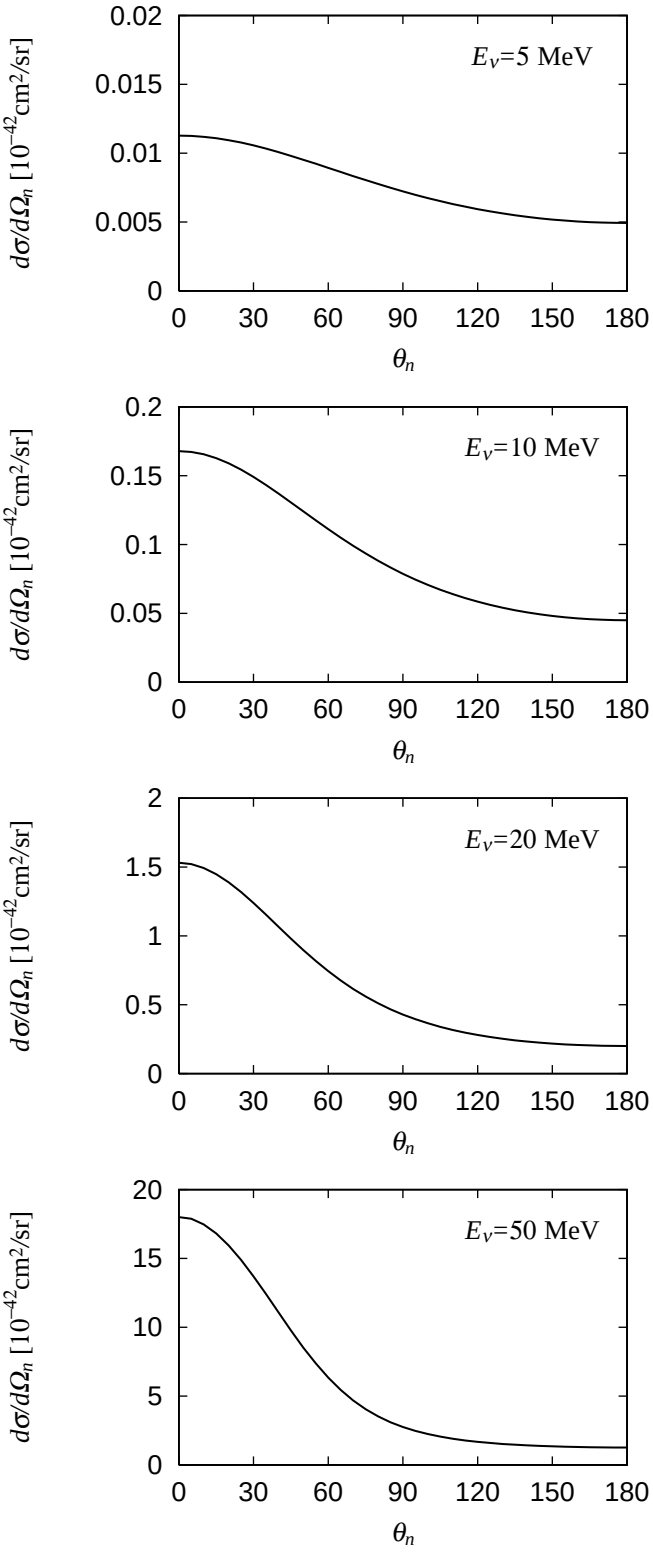

FIG. 6. Neutron angular distribution for the $\nu d \to \nu pn$ reaction.

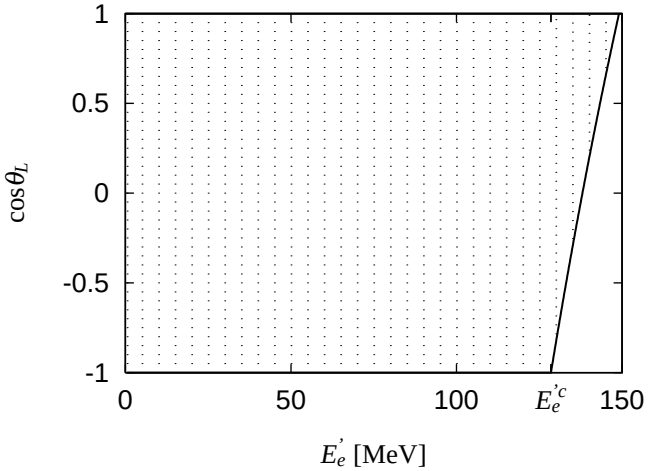

FIG. 7. Kinematically allowed region of the electron scattering angle θ_L in the $\nu_e d \to e^- pp$ reaction at $E_\nu = 150$ MeV. The dotted area represents the allowed region. The constraint on θ_L sets in at $E'_e = E'^c_e$.

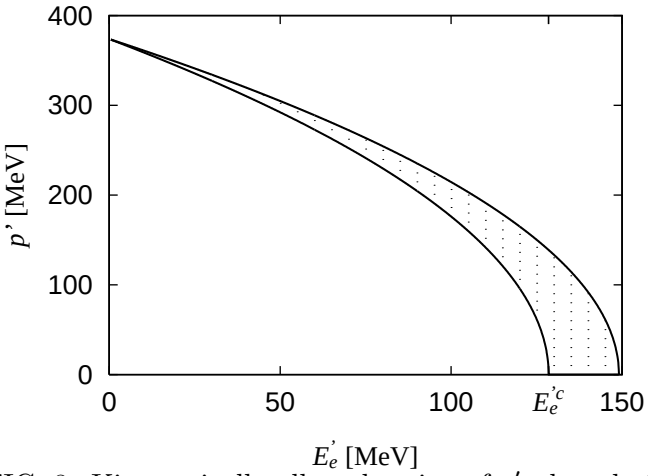

FIG. 8. Kinematically allowed region of p', the relative momentum of the final two nucleons in the $\nu_e d \to e^- pp$ reaction at $E_\nu = 150$ MeV. The lower limit of p' reaches zero at $E'_e = E'^c_e$.